Fully Uncalibrated Image-Based Visual Servoing of 2DOFs Planar Manipulators With a Fixed Camera

Xinwu Liang, *Member, IEEE*, Hesheng Wang, *Senior Member, IEEE*, Yun-Hui Liu, *Fellow, IEEE*, Bing You, Zhe Liu, Zhongliang Jing, *Senior Member, IEEE*, and Weidong Chen, *Member, IEEE*

***Abstract*—We consider the uncalibrated vision-based control problem of robotic manipulators in this work. Though lots of approaches have been proposed to solve this problem, they usually require calibration (offline or online) of the camera parameters in the implementation, and the control performance may be largely affected by parameter estimation errors. In this work, we present new fully uncalibrated visual servoing approaches for position control of the 2DOFs planar manipulator with a fixed camera. In the proposed approaches, no camera calibration is required, and numerical optimization algorithms or adaptive laws for parameter estimation are not needed. One benefit of such features is that exponential convergence of the image position errors can be ensured regardless of the camera parameter uncertainties. Generally, existing uncalibrated approaches only can guarantee asymptotical convergence of the position errors. Moreover, different from most existing approaches which assume that the robot motion plane and the image plane are parallel, one of the proposed approaches allows the camera to be installed at a general pose. This also simplifies the controller implementation and improves the system design flexibility. Finally, simulation and experimental results are provided to illustrate the effectiveness of the presented fully uncalibrated visual servoing approaches.**

***Index Terms*—Fully uncalibrated camera, image-based visual servoing (IBVS), image Jacobian, robotic manipulator.**

Manuscript received 26 January 2021; accepted 26 March 2021. Date of publication 28 April 2021; date of current version 16 September 2022. This work was supported in part by the Natural Science Foundation of China under Grant U1813219, Grant 62073222, Grant U1913204, and Grant 61673272; and in part by the Shenzhen Science and Technology Innovation Commission under Grant KQTD20140630150243062. This article was recommended by Associate Editor H. Qiao. *(Corresponding author: Hesheng Wang.)*

Xinwu Liang and Zhongliang Jing are with the School of Aeronautics and Astronautics, Shanghai Jiao Tong University, Shanghai 200240, China (e-mail: xinwu113@163.com; zljing@sjtu.edu.cn).

Hesheng Wang and Weidong Chen are with the Department of Automation, Institute of Medical Robotics, Key Laboratory of System Control and Information Processing of Ministry of Education, Shanghai Jiao Tong University, Shanghai 200240, China (e-mail: wanghesheng@sjtu.edu.cn; wdchen@sjtu.edu.cn).

Yun-Hui Liu is with the Department of Mechanical and Automation Engineering, The Chinese University of Hong Kong, Hong Kong (e-mail: yhliu@mae.cuhk.edu.hk).

Bing You is with the Maintenance Department III, Fujian Fuqing Nuclear Power Company, Ltd., Fuqing 350300, China (e-mail: youbing01@cnnp.com.cn).

Zhe Liu is with the Department of Computer Science and Technology, University of Cambridge, Cambridge CB3 0FD, U.K. (e-mail: zl457@cam.ac.uk).

Color versions of one or more figures in this article are available at https://doi.org/10.1109/TCYB.2021.3070598.

Digital Object Identifier 10.1109/TCYB.2021.3070598

I. Introduction

VISUAL servoing is a useful technique that can be used to establish an efficient, flexible, reliable, and high-performance closed-loop servo system for controlling the motion of robots. Up to now, many different visual servoing approaches [1], which can be mainly classified as position-based visual servoing (PBVS), image-based visual servoing (IBVS), and hybrid visual servoing (HVS) approaches, have been proposed to control the motion of robotic manipulators [2]–[5], mobile robots [6]–[8], and underwater vehicles [9].

Considering that camera calibration is time consuming and error prone in the presence of measurement noises or due to changes in working conditions and usually obtaining accurate camera parameters is very difficult, a critical issue to be handled in the design of a visual servo system is the potential uncertainty in the camera parameters. It is well known that in PBVS schemes, the camera calibration errors directly result in pose estimation errors and finally lead to task errors, which means that tedious camera calibration is required to obtain accurate camera parameters to achieve high control accuracy of a PBVS approach. Compared to PBVS schemes, HVS schemes are more robust to camera calibration errors, but since the camera calibration errors still can affect the accuracy of partial pose reconstruction, it is recommended to use camera parameters with sufficient accuracy for the design of an HVS approach to guarantee the desired attraction domain and good transient behavior. This implies that coarse camera calibration is often necessary for HVS schemes. Though IBVS schemes are particularly robust to errors in the camera calibration, too large parameter errors can make the performance deteriorate significantly and may lead to system instability. With this in mind, coarse camera calibration is also needed in the design of an IBVS approach to ensure satisfactory performance. Hence, usually, the camera parameters need to be calibrated with enough precision to achieve high visual servo performance.

A. Model-Free Uncalibrated Visual Servoing

To avoid tedious camera calibration, improve the control performance when only coarse or bad camera parameters are available, or realize an effective servo task when users have poor or no priori knowledge of the system model/parameters with no camera calibration, various uncalibrated visual servoing approaches that have been proposed for

coping with the parameter uncertainty arising from the camera system.

1) Numerical Optimization-Based Approaches: In [10], an uncalibrated visual servoing approach without priori knowledge about the system parameters or the kinematic structure was proposed, where the image Jacobian was estimated based on the weighted recursive least-square (RLS) method. In [11], the *Broyden* method was adopted to recursively update the Jacobian. In [12], an uncalibrated visual servoing approach based on the exploratory motion was proposed to improve the estimation of the image Jacobian. To achieve efficient tracking of moving targets with a fixed camera, an RLS Jacobian estimation-based dynamic *quasi-Newton* method was presented in [13]. In [14], nonrecursive and recursive *Gauss-Newton* controllers with a partitioned *Broyden* Jacobian estimation algorithm were formulated to handle the eye-in-hand tracking problem of moving targets. In [15], a statistically robust M-estimator was applied for estimating the Jacobian matrix to improve the estimation quality. In [16], an uncalibrated iterative-learning-control-based visual servoing approach was proposed, where the image Jacobian is iteratively estimated using the neural network approximation method. In [17], several *Broyden*-type Jacobian estimation-based uncalibrated visual servoing approaches were analyzed in a unified framework. In [18], an extended state observer was proposed for the online estimation of the Jacobian modeling error but not the Jacobian itself. To overcome the drawback of local Jacobian estimation schemes, two global Jacobian estimators were proposed in [19] based on the robot movement history. The image Jacobian is known to be a locally linear approximation of the nonlinear visual-motor model. In [20], the nonlinear visual-motor model was estimated based on the offline training of a neural network.

2) Machine Learning-Based Approaches: In [21], two reinforcement learning methods were proposed to address the uncalibrated visual servoing problem. To improve the control performance and enhance the robustness with respect to calibration/modeling errors, a neural network reinforcement learning controller was designed in [22]. In [23], a visual servo system based on the neural fitted Q-iteration method was developed to solve a combined reaching and grasping task. To reduce the number of training samples and the learning time, a self-learning visual servo system was proposed in [24] using Q-learning and fuzzy neural network algorithms. In [25], a learning visual servoing framework was presented by combining learned image features, learned dynamic models, and the fitted Q-iteration algorithm. A visual servo system using Gaussian mixture model-based machine learning was presented in [26]. In [27], an end-to-end learning framework based on convolutional neural networks (CNNs) was proposed to address the uncalibrated PBVS problem. This framework was extended in [28] by repurposing pretrained CNNs.

The most attractive feature of the model-free uncalibrated visual servoing approaches is that the linear/nonlinear visual-motor model is estimated online or learned offline and, hence, the explicit derivation of an analytical kinematic model can be avoided, and direct camera calibration is not necessary.

B. Model-Based Uncalibrated Visual Servoing

Explicit derivation of an analytical parametric visual-motor model can increase the design complexity of a visual servo system, but generally, it can be taken as a prerequisite step for achieving high control performance. When the parametric visual-motor model is used for the design of a visual servo system, in uncalibrated environments, one has to develop adaptive laws for camera parameter estimation and depth compensation. To address these issues, many model-based uncalibrated visual servoing approaches have been developed.

1) Approaches for the Case With Constant Feature Depths: In [29], an adaptive visual servoing approach was presented for tracking control of planar manipulators using a fixed camera. A tracking controller, which can handle the parameter uncertainty in the entire robot-camera system and can guarantee globally asymptotical tracking without imposing any persistently exciting condition to the desired trajectory, was presented in [30]. To avoid overparametrization, projections, and persistency of excitation assumptions, adaptive position controllers were developed in [31] and [32]. The results in [32] were extended in [33] to consider the robot dynamics. In [34], a two-layered visual servoing controller was developed to address the trajectory tracking control issue of 2DOFs planar manipulators with uncertain dynamics and camera parameters. To ensure globally asymptotical convergence of the tracking errors without overparameterization, adaptive visual servoing controllers were presented in [35]. In [36], the proportional actuator model uncertainty was considered besides the uncertain camera, kinematic, and dynamic parameters. To simultaneously handle uncertainties in kinematics as well as rigid-body and actuator dynamics, an adaptive tracking controller was proposed in [37]. In [38], the adaptive regulation problem of robotic manipulators with actuator saturation constraints was addressed. To avoid performance degradation caused by velocity measurement noise, a tracking controller was designed in [39] without joint-space and task-space velocity measurements.

2) Approaches for the Case With Time-Varying Feature Depths: The previously mentioned model-based uncalibrated visual servoing approaches in [29]–[39] can only be applied to the case with constant or slowly time-varying feature depths. Hence, to use the approaches in [29]–[39], the camera needs to be mounted such that the motion plane of the feature point and the image plane are parallel. To make a visual servo controller more practical and applicable to wider application domains, it is required to develop uncalibrated controllers without the parallelism requirement. To solve this problem, model-based uncalibrated visual servoing schemes have been developed without such a requirement. In [40], an adaptive uncalibrated HVS control scheme was proposed to address the 6DOFs regulation problem. An adaptive IBVS controller was presented in [41] by introducing the depth-independent interaction matrix framework. This framework was applied to tackle the tracking control problem in [42], which was improved in [43] by designing adaptive laws with guaranteed stability. This framework was further used in [44] to address the eye-in-hand uncalibrated IBVS problem. The controllers in [41]–[44]

can deal with uncertainties in the camera parameters, but the effects of uncertain robot kinematics and dynamics were not considered. In [45], an adaptive IBVS control scheme was proposed to solve the regulation problem with uncertain depth, camera intrinsic and extrinsic, kinematic, and dynamic parameters. To avoid the overparametrization problem in the depth-independent interaction matrix framework, an observer-based adaptive tracking controller without image velocity measurements was presented in [46]. The uncalibrated controllers in [40]–[46] were proposed for one of the fixed and eye-in-hand camera configurations. In [47], a unified design approach, which can be used for both camera configurations, was proposed for the tracking control problem.

C. Motivation

Though so many uncalibrated vision-based control schemes have been developed for robotic manipulators, including model-free and model-based uncalibrated approaches, they do not belong to fully uncalibrated vision-based control schemes, which require neither offline nor online camera calibration. Offline precise camera calibration can be avoided in existing uncalibrated schemes, but online calibration is necessary. In the model-free uncalibrated approaches, online indirect camera calibration or offline model learning is needed, where numerical optimization algorithms or machine learning techniques are used to estimate the camera-parameter-dependent elements in the visual-motor model or learn the model itself. In the model-based uncalibrated approaches, online direct camera calibration is required, where adaptive laws are designed to estimate the camera parameters. Regardless of the kind of camera calibration strategy (the indirect or direct one) we adopt, typically, a rough initial estimation of the camera parameters/visual-motor model or an efficient training dataset should be available to guarantee satisfactory performance. However, when initial values are far from the true ones or the training dataset is not representative enough, the convergence rate for the estimation of the camera parameters or learning of the visual-motor model will be slow, and the control performance will deteriorate, which may cause the manipulator to move erroneously and finally lead to task failure. Hence, usually, adequate priori knowledge about the camera parameters or enough training data is required for the design of existing uncalibrated visual servoing approaches to achieve high control performance. If one can develop a fully uncalibrated visual servoing approach, due to the absence of offline and online camera calibration/model learning, high-performance control of robotic manipulators can be achieved with no priori information about the camera parameters and without the need to handle the tedious data gathering task, which is theoretically and practically appealing and is our main objective in this work.

D. Contribution and Novelty

In this work, we develop fully uncalibrated IBVS approaches for 2DOFs planar manipulators with a fixed camera. In the developed approaches, any priori knowledge of the camera parameters is not necessary, and a completely unknown camera can be used for controller design.

Though the developed approaches share the same motivation as our previous works in [48]–[50], that is, to totally eliminate offline and online camera calibration from the visual servo controller design, there exist many differences between them. The approaches in [48]–[50] were proposed for mobile robots, whereas the current work is to address the fully uncalibrated visual servoing problem of robotic manipulators. IBVS for mobile robots and robotic manipulators is, in principle, similar in the sense that their controllers are developed by mapping the image space errors to the control space. Nevertheless, the controller design for them have some major differences. One important difference is that nonholonomic constraints exist in the motion of mobile robots, while this is not the case for robotic manipulators. This can make the controller design of mobile robots different from that of robotic manipulators. Furthermore, though general forms of the image Jacobian matrices for both types of robotic systems might look similar at first glance, they are quite different after analyzing their detailed expressions. These differences imply that the approaches in [48]–[50] are not directly applicable to robotic manipulators. Actually, it is impossible to design an IBVS controller for a robotic manipulator if we do not derive its image-space kinematic model, whose main purpose is to obtain the image Jacobian. To solve the fully uncalibrated visual servoing problem of robotic manipulators, it is necessary to derive the image Jacobian independent of the camera parameters.

It will be shown that by using two additional particular feature points, the image Jacobian for the 2DOFs planar manipulators with a fixed camera can be rewritten into a new form without depending on the camera parameters, which is a key finding in the current work. Though the number of feature points used for the 2DOFs planar manipulators is the same as that adopted for mobile robots in [48]–[50], their arrangements are very different. This also implies that the current work is not a trivial extension of our previous works [48]–[50]. As can be seen from the development in this article, derivation of the desired image-space kinematic model for the 2DOFs planar manipulators is more complicated, and the finally obtained camera-parameter-independent image Jacobian is different, compared with the case of mobile robots. This further reflects the fact that the approaches in [48]–[50] cannot be trivially applied to robotic manipulators, and shows the necessity and the value of the model development in this article. In conclusion, to the best of our knowledge, the developed approaches are the first ones that can be used to deal with the fully uncalibrated visual servoing problem of robotic manipulators.

The novel contributions in this work can be summarized as: 1) a new kinematic model in the image space is developed for the 2DOFs planar manipulator with a fixed camera. Completely different from the existing ones, the camera parameters are successfully removed from the developed model by introducing additional feature points and 2) two novel IBVS controllers, which are, respectively, based on the depth-ratio-based and depth-free image Jacobian matrices, are proposed for position control of the 2DOFs planar

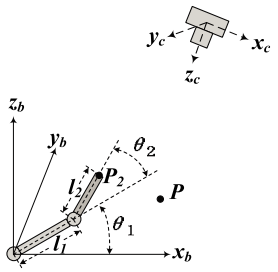

Fig. 1. Robot-camera system configuration for the 2DOFs planar robotic manipulator with a fixed camera.

manipulator without any camera calibration. The uncalibrated visual servoing problem of planar manipulators has attracted much attention in the past two decades, and lots of approaches [29]–[35] have been presented. However, these approaches have a common drawback that the camera needs to be fixed perpendicular to the robot motion plane, and many of them impose restrictive conditions on the camera orientation. Furthermore, these approaches need to design adaptive laws to handle the adaptive camera calibration problem and typically require priori information about the camera parameters for efficient parameter estimation. In contrast, a notable feature of the developed approaches in this work is that the camera can be mounted without the parallelism requirement and without the assumption about camera orientation. Moreover, the design of optimization algorithms/adaptive laws for online camera calibration or the tedious machine learning-based training for offline model estimation is not needed, and no priori information about the camera parameters or no data collection is necessary. Finally, different from most existing uncalibrated approaches, which only ensure asymptotical error convergence, exponential error convergence is guaranteed by the developed approaches, which therefore can be used for achieving high-performance control of planar manipulators even with a totally unknown camera.

II. Preliminaries

A. Perspective Projection Model

We consider a 2DOFs robotic manipulator that moves in a plane in this work. We assume that a pinhole camera is mounted above the workspace of the robotic manipulator, and the system configuration is presented in Fig. 1. As shown in Fig. 1, to facilitate subsequent development, two coordinate frames: 1) the camera coordinate frame C and 2) the robot base coordinate frame B, are defined. The motion plane of the manipulator and xy plane of the robot base coordinate frame coincide. The lengths of the first and second links of the planar manipulator are denoted by l_1 and l_2, and the angles of the first and second joints are defined as θ_1 and θ_2, respectively.

For convenience, we consider a general feature point P in the motion plane and here present its perspective projection model. Planar coordinates of the feature point P are denoted by $\boldsymbol{x}_p \in \Re^{2\times 1}$, expressed in the coordinate frame B. Denote the homogenous transformation matrix between the coordinate frames B and C by $\mathbf{T}_B^C \in \Re^{4\times 4}$, which is the camera extrinsic matrix. Using the coordinate transformation, the homogeneous coordinates $\boldsymbol{x}_p^C \in \Re^{4\times 1}$ of the feature point P are derived as

$$\boldsymbol{x}_p^C = \mathbf{T}_B^C \begin{bmatrix} \boldsymbol{x}_p \\ 0 \\ 1 \end{bmatrix} = \begin{bmatrix} \mathbf{R}_B^C & \boldsymbol{t}_B^C \\ \mathbf{0}_{1\times 3} & 1 \end{bmatrix} \begin{bmatrix} \boldsymbol{x}_p \\ 0 \\ 1 \end{bmatrix} \tag{1}$$

which is expressed in the camera coordinate frame. Note that $\boldsymbol{t}_B^C \in \Re^{3\times 1}$ and $\mathbf{R}_B^C \in \Re^{3\times 3}$ represent the translational and rotational components of the matrix $\mathbf{T}_B^C$. Under the pinhole camera model, image coordinates $\boldsymbol{y}_p = (u_p, v_p)^\top \in \Re^{2\times 1}$ of the feature point P are expressed as

$$\begin{bmatrix} \boldsymbol{y}_p \\ 1 \end{bmatrix} = \frac{1}{z_p^C} \begin{bmatrix} \mathbf{A} & \mathbf{0}_{3\times 1} \end{bmatrix} \boldsymbol{x}_p^C \tag{2}$$

where z_p^C is the depth of the feature point P, and $\mathbf{A} \in \Re^{3\times 3}$ is the camera intrinsic matrix. Substituting (1) into (2) yields

$$\begin{bmatrix} \boldsymbol{y}_p \\ 1 \end{bmatrix} = \frac{1}{z_p^C} \mathbf{H} \begin{bmatrix} \boldsymbol{x}_p \\ 1 \end{bmatrix} \tag{3}$$

where $\mathbf{H} = \mathbf{A}[\boldsymbol{r}_1\ \boldsymbol{r}_2\ \boldsymbol{t}_B^C] \in \Re^{3\times 3}$ denotes the homography matrix, which is determined by the camera intrinsic and extrinsic parameters, and $\boldsymbol{r}_i$ is the ith column of $\mathbf{R}_B^C$. Based on (3), the depth of the feature point P and its image coordinates are compactly rewritten as

$$z_p^C = \boldsymbol{h}_3^\top \begin{bmatrix} \boldsymbol{x}_p \\ 1 \end{bmatrix} \tag{4}$$

$$\boldsymbol{y}_p = \frac{1}{z_p^C} \begin{bmatrix} \boldsymbol{h}_1^\top \\ \boldsymbol{h}_2^\top \end{bmatrix} \begin{bmatrix} \boldsymbol{x}_p \\ 1 \end{bmatrix} \tag{5}$$

where $\boldsymbol{h}_i^\top \in \Re^{1\times 3}$ denotes the ith row of $\mathbf{H}$.

B. Image-Space Kinematic Model

For the visual servoing task considered in this work, the objective is to move the feature point P_2, which is attached on the robot tip, such that it can reach a desired image position. To do that, we need to develop an image-space kinematic model of the robotic manipulator associated with the feature point P_2. The expressions of the depth of the feature point P_2 and its image coordinates z_{p2}^C and $\boldsymbol{y}_{p2} = (u_{p2}, v_{p2})^\top$ can be derived based on (4) and (5) by replacing the coordinates $\boldsymbol{x}_p$ with the planar coordinates $\boldsymbol{x}_{p2} \in \Re^{2\times 1}$ of the feature point P_2

$$z_{p2}^C = \boldsymbol{h}_3^\top \begin{bmatrix} \boldsymbol{x}_{p2} \\ 1 \end{bmatrix} \tag{6}$$

$$z_{p2}^C u_{p2} = \boldsymbol{h}_1^\top \begin{bmatrix} \boldsymbol{x}_{p2} \\ 1 \end{bmatrix} \tag{7}$$

$$z_{p2}^C v_{p2} = \boldsymbol{h}_2^\top \begin{bmatrix} \boldsymbol{x}_{p2} \\ 1 \end{bmatrix}. \tag{8}$$

The planar coordinates $\boldsymbol{x}_{p2}$ can be directly obtained based on the manipulator forward kinematics

$$\boldsymbol{x}_{p2} = \begin{bmatrix} l_1 c_1 + l_2 c_{12} \\ l_1 s_1 + l_2 s_{12} \end{bmatrix}$$

where we have used the notations $\cos\theta_1 \triangleq c_1$, $\sin\theta_1 \triangleq s_1$, $\cos(\theta_1+\theta_2) \triangleq c_{12}$ and $\sin(\theta_1+\theta_2) \triangleq s_{12}$ for simplicity. Differentiating (7) and (8) with respect to time results in

$$\dot{\boldsymbol{y}}_{p2} = -\frac{\dot{z}_{p2}^C}{z_{p2}^C} \frac{1}{z_{p2}^C} \begin{bmatrix} \boldsymbol{h}_1^\top \\ \boldsymbol{h}_2^\top \end{bmatrix} \begin{bmatrix} \boldsymbol{x}_{p2} \\ 1 \end{bmatrix} + \frac{1}{z_{p2}^C} \begin{bmatrix} \boldsymbol{h}_1^\top \\ \boldsymbol{h}_2^\top \end{bmatrix} \begin{bmatrix} \dot{\boldsymbol{x}}_{p2} \\ 0 \end{bmatrix}. \tag{9}$$

Substituting (7), (8), and the time derivative of z_{p2}^C into (9), we have

$$\dot{\boldsymbol{y}}_{p2} = \frac{1}{z_{p2}^C}\left\{\begin{bmatrix}\boldsymbol{h}_1^\top \\ \boldsymbol{h}_2^\top\end{bmatrix} - \boldsymbol{y}_{p2}\boldsymbol{h}_3^\top\right\}\begin{bmatrix}\dot{\boldsymbol{x}}_{p2} \\ 0\end{bmatrix}. \tag{10}$$

Differentiating $\boldsymbol{x}_{p2}$ with respect to time, the differential kinematics of the robotic manipulator can be obtained as

$$\dot{\boldsymbol{x}}_{p2} = \begin{bmatrix}-l_1 s_1 - l_2 s_{12} & -l_2 s_{12} \\ l_1 c_1 + l_2 c_{12} & l_2 c_{12}\end{bmatrix}\begin{bmatrix}\dot{\theta}_1 \\ \dot{\theta}_2\end{bmatrix} \triangleq \mathbf{J}_r\begin{bmatrix}\dot{\theta}_1 \\ \dot{\theta}_2\end{bmatrix} \tag{11}$$

where $\mathbf{J}_r \in \Re^{2\times 2}$ denotes the analytical Jacobian of the 2DOFs planar manipulator. Substituting (11) into (10) leads to the following kinematic model of the planar manipulator in the image space:

$$\dot{\boldsymbol{y}}_{p2} = \frac{1}{z_{p2}^C}\begin{bmatrix}g_{11} & g_{12} \\ g_{21} & g_{22}\end{bmatrix}\begin{bmatrix}\dot{\theta}_1 \\ \dot{\theta}_2\end{bmatrix} \triangleq \frac{1}{z_{p2}^C}\mathbf{G}_{p2}\begin{bmatrix}\dot{\theta}_1 \\ \dot{\theta}_2\end{bmatrix} \tag{12}$$

where $\mathbf{G}_{p2} \in \Re^{2\times 2}$ represents the depth-independent image Jacobian of the 2DOFs planar manipulator, and

$$\begin{aligned} g_{11} &= h_{11}(-l_1 s_1 - l_2 s_{12}) + h_{12}(l_1 c_1 + l_2 c_{12}) \\ &\quad - u_{p2}\{h_{31}(-l_1 s_1 - l_2 s_{12}) + h_{32}(l_1 c_1 + l_2 c_{12})\} \quad (13) \\ g_{12} &= h_{11}(-l_2 s_{12}) + h_{12}(l_2 c_{12}) \\ &\quad - u_{p2}\{h_{31}(-l_2 s_{12}) + h_{32}(l_2 c_{12})\} \quad (14) \\ g_{21} &= h_{21}(-l_1 s_1 - l_2 s_{12}) + h_{22}(l_1 c_1 + l_2 c_{12}) \\ &\quad - v_{p2}\{h_{31}(-l_1 s_1 - l_2 s_{12}) + h_{32}(l_1 c_1 + l_2 c_{12})\} \quad (15) \\ g_{22} &= h_{21}(-l_2 s_{12}) + h_{22}(l_2 c_{12}) \\ &\quad - v_{p2}\{h_{31}(-l_2 s_{12}) + h_{32}(l_2 c_{12})\} \quad (16) \end{aligned}$$

with h_{ij} being the ith row and jth column element of $\mathbf{H}$.

C. Problem Statement

When the image-space kinematic model (12) is employed to develop visual servo controllers for the 2DOFs planar manipulator, we need to use offline calibration methods to identify the camera parameters or numerical-optimization/adaptive-estimation-based online calibration approaches to compensate for their uncertainties. The visual servoing problem of the planar manipulator without offline or online camera calibration cannot be addressed based on the model (12), due to the existence of the camera parameters. In this work, our objective is to provide feasible solutions to such a problem.

Problem 1: Given a desired image position $\boldsymbol{y}_{p2}^d = (u_{p2}^d, v_{p2}^d)^\top$ of P_2, design control inputs $(\dot{\theta}_1, \dot{\theta}_2)$ for the 2DOFs planar manipulator based on image feedback from a fixed camera such that the feature point P_2 is regulated to the desired image position, that is, the image position error $\Delta\boldsymbol{y}_{p2} = \boldsymbol{y}_{p2} - \boldsymbol{y}_{p2}^d \to \mathbf{0}$ as $t \to \infty$, without online or offline calibration of the camera intrinsic and extrinsic parameters.

To address Problem 1, it is necessary to derive a new image-space kinematic model without explicitly depending on the camera parameters. This is our task in the next section.

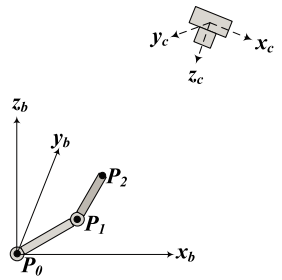

Fig. 2. Robot-camera system configuration in the proposed image-space kinematic model.

III. Proposed Image-Space Kinematic Model

To make it possible to develop an image-space kinematic model with desired properties, three feature points are used in the system. In other words, besides the feature point P_2 for the task specification, two additional feature points: 1) the feature point P_1 (attached at the second joint axis of the manipulator) and 2) the feature point P_0 (attached at the first joint axis) as shown in Fig. 2, are adopted to facilitate the model development.

The planar coordinates $\boldsymbol{x}_{p1} \in \Re^{2\times 1}$ of P_1, expressed in the coordinate frame B, are given by

$$\boldsymbol{x}_{p1} = \begin{bmatrix}l_1 c_1 \\ l_1 s_1\end{bmatrix}.$$

Then, from the general projection model in (4) and (5), the depth z_{p1}^C of the feature point P_1 and its image coordinates $\boldsymbol{y}_{p1} = (u_{p1}, v_{p1})^\top$ are expressed as

$$z_{p1}^C = \boldsymbol{h}_3^\top\begin{bmatrix}\boldsymbol{x}_{p1} \\ 1\end{bmatrix} \tag{17}$$

$$z_{p1}^C u_{p1} = \boldsymbol{h}_1^\top\begin{bmatrix}\boldsymbol{x}_{p1} \\ 1\end{bmatrix} \tag{18}$$

$$z_{p1}^C v_{p1} = \boldsymbol{h}_2^\top\begin{bmatrix}\boldsymbol{x}_{p1} \\ 1\end{bmatrix}. \tag{19}$$

Moreover, the planar coordinates $\boldsymbol{x}_{p0} \in \Re^{2\times 1}$ of P_0, expressed in the robot base frame, can be written as

$$\boldsymbol{x}_{p0} = \begin{bmatrix}0 \\ 0\end{bmatrix}.$$

Similarly, the depth z_{p0}^C of the feature point P_0 and its image coordinates $\boldsymbol{y}_{p0} = (u_{p0}, v_{p0})^\top$ are given by

$$z_{p0}^C = \boldsymbol{h}_3^\top\begin{bmatrix}\boldsymbol{x}_{p0} \\ 1\end{bmatrix} \tag{20}$$

$$z_{p0}^C u_{p0} = \boldsymbol{h}_1^\top\begin{bmatrix}\boldsymbol{x}_{p0} \\ 1\end{bmatrix} \tag{21}$$

$$z_{p0}^C v_{p0} = \boldsymbol{h}_2^\top\begin{bmatrix}\boldsymbol{x}_{p0} \\ 1\end{bmatrix}. \tag{22}$$

Next, we will use image coordinates of P_2, P_1 and P_0 and their depths to develop the desired image-space kinematic model, which is achieved via deriving new representations of g_{11}, g_{12}, g_{21}, and g_{22}.

A. New Representations of g_{11} and g_{12}

As usually done in the literature, in our study, it is assumed that kinematic singularities related to the analytical Jacobian $\mathbf{J}_r$ can be avoided. Based on this assumption, the determinant of $\mathbf{J}_r$ is nonzero, and we have $s_2 \triangleq \sin\theta_2 \neq 0$ since $\det \mathbf{J}_r = l_1 l_2 s_2$. In subsequent development, the following relationship plays an important role in deriving the new image-space kinematic model:

$$l_2^2(l_1^2 + 2l_1l_2c_2 + l_2^2) - \left(l_2^2 + l_1l_2c_2\right)\left(l_2^2 + l_1l_2c_2\right) = l_1^2l_2^2s_2^2 \tag{23}$$

where $c_2 \triangleq \cos\theta_2$.

Based on the relationship (23) and considering the nonzero property of s_2, g_{11} can be rewritten as

$$g_{11} = \frac{1}{l_1^2l_2^2s_2^2}\Big\{g_{11}l_2^2\left(l_1^2 + 2l_1l_2c_2 + l_2^2\right) - g_{11}\left(l_2^2 + l_1l_2c_2\right)\left(l_2^2 + l_1l_2c_2\right)\Big\}. \tag{24}$$

By adding and subtracting $g_{12}(l_2^2 + l_1l_2c_2)(l_1^2 + 2l_1l_2c_2 + l_2^2)$ inside the brace and then rearranging and combining the like terms, (24) can be reexpressed as

$$g_{11} = \frac{1}{l_1^2l_2^2s_2^2}\left\{\bar{g}_{11}\left(l_2^2 + l_1l_2c_2\right) + \bar{g}_{12}\left(l_1^2 + 2l_1l_2c_2 + l_2^2\right)\right\} \tag{25}$$

where $\bar{g}_{11}$ and $\bar{g}_{12}$ are, respectively, defined as

$$\bar{g}_{11} = -g_{11}\left(l_2^2 + l_1l_2c_2\right) + g_{12}\left(l_1^2 + 2l_1l_2c_2 + l_2^2\right) \tag{26}$$

$$\bar{g}_{12} = g_{11}l_2^2 - g_{12}\left(l_2^2 + l_1l_2c_2\right). \tag{27}$$

Substituting (13) and (14) into (26), with some simple manipulations, we have

$$\bar{g}_{11} = h_{11}\Psi_1 - h_{12}\Psi_2 + u_{p2}(-h_{31}\Psi_1 + h_{32}\Psi_2) \tag{28}$$

where Ψ_1 and Ψ_2 are given by

$$\Psi_1 = l_1l_2^2s_1 + l_1^2l_2s_1c_2 - l_1^2l_2s_{12} - l_1l_2^2c_2s_{12}$$
$$\Psi_2 = l_1l_2^2c_1 + l_1^2l_2c_1c_2 - l_1^2l_2c_{12} - l_1l_2^2c_2c_{12}.$$

Based on the fact that $s_{12} = s_1c_2 + c_1s_2$, Ψ_1 can be finally simplified as

$$\Psi_1 = -l_1l_2s_2(l_1c_1 + l_2c_{12}). \tag{29}$$

While by using the relationship $c_{12} = c_1c_2 - s_1s_2$, Ψ_2 can be reduced to

$$\Psi_2 = l_1l_2s_2(l_1s_1 + l_2s_{12}). \tag{30}$$

Substituting (29) and (30) into (28) yields

$$\bar{g}_{11} = -l_1l_2s_2\big\{h_{11}(l_1c_1 + l_2c_{12}) + h_{12}(l_1s_1 + l_2s_{12}) - u_{p2}[h_{31}(l_1c_1 + l_2c_{12}) + h_{32}(l_1s_1 + l_2s_{12})]\big\}. \tag{31}$$

According to the definitions of $\boldsymbol{x}_{p2}$ and $\boldsymbol{x}_{p0}$, we can obtain

$$h_{11}(l_1c_1 + l_2c_{12}) + h_{12}(l_1s_1 + l_2s_{12}) = \boldsymbol{h}_1^\top\left\{\begin{bmatrix}\boldsymbol{x}_{p2}\\1\end{bmatrix} - \begin{bmatrix}\boldsymbol{x}_{p0}\\1\end{bmatrix}\right\} = z_{p2}^Cu_{p2} - z_{p0}^Cu_{p0} \tag{32}$$

where (7) and (21) have been used. Similarly, it is easy to show that

$$h_{31}(l_1c_1 + l_2c_{12}) + h_{32}(l_1s_1 + l_2s_{12}) = \boldsymbol{h}_3^\top\left\{\begin{bmatrix}\boldsymbol{x}_{p2}\\1\end{bmatrix} - \begin{bmatrix}\boldsymbol{x}_{p0}\\1\end{bmatrix}\right\} = z_{p2}^C - z_{p0}^C \tag{33}$$

where (6) and (20) are applied. Substituting (32) and (33) into (31) leads to

$$\bar{g}_{11} = -l_1l_2s_2z_{p0}^C(u_{p2} - u_{p0}). \tag{34}$$

Substituting (13) and (14) into (27), $\bar{g}_{12}$ is expressed as

$$\bar{g}_{12} = -h_{11}\Psi_3 + h_{12}\Psi_4 + u_{p2}(h_{31}\Psi_3 - h_{32}\Psi_4) \tag{35}$$

where

$$\Psi_3 = l_1l_2^2s_1 - l_1l_2^2c_2s_{12}$$
$$\Psi_4 = l_1l_2^2c_1 - l_1l_2^2c_2c_{12}.$$

Considering that $s_{12} = s_1c_2 + c_1s_2$ and $c_{12} = c_1c_2 - s_1s_2$, Ψ_3 and Ψ_4 can be further transformed as follows:

$$\Psi_3 = -l_1l_2s_2(l_2c_{12}) \tag{36}$$

$$\Psi_4 = l_1l_2s_2(l_2s_{12}). \tag{37}$$

Substituting (36) and (37) into (35) results in

$$\bar{g}_{12} = l_1l_2s_2\big\{h_{11}(l_2c_{12}) + h_{12}(l_2s_{12}) - u_{p2}[h_{31}(l_2c_{12}) + h_{32}(l_2s_{12})]\big\}. \tag{38}$$

Based on the definitions of $\boldsymbol{x}_{p2}$ and $\boldsymbol{x}_{p1}$, we have

$$h_{11}(l_2c_{12}) + h_{12}(l_2s_{12}) = \boldsymbol{h}_1^\top\left\{\begin{bmatrix}\boldsymbol{x}_{p2}\\1\end{bmatrix} - \begin{bmatrix}\boldsymbol{x}_{p1}\\1\end{bmatrix}\right\} = z_{p2}^Cu_{p2} - z_{p1}^Cu_{p1} \tag{39}$$

where we have used (7) and (18). In the same way, we can derive that

$$h_{31}(l_2c_{12}) + h_{32}(l_2s_{12}) = \boldsymbol{h}_3^\top\left\{\begin{bmatrix}\boldsymbol{x}_{p2}\\1\end{bmatrix} - \begin{bmatrix}\boldsymbol{x}_{p1}\\1\end{bmatrix}\right\} = z_{p2}^C - z_{p1}^C \tag{40}$$

where (6) and (17) have been applied. Substituting (39) and (40) into (38), one arrives at

$$\bar{g}_{12} = l_1l_2s_2z_{p1}^C(u_{p2} - u_{p1}). \tag{41}$$

Now, substituting (34) and (41) into (25), g_{11} can be finally transformed into the following form:

$$g_{11} = \frac{1}{l_1l_2s_2}\Big\{\left(l_1^2 + 2l_1l_2c_2 + l_2^2\right)z_{p1}^C(u_{p2} - u_{p1}) - \left(l_2^2 + l_1l_2c_2\right)z_{p0}^C(u_{p2} - u_{p0})\Big\}. \tag{42}$$

Next, we will derive the new representation of g_{12}.

Through the use of (23), g_{12} can be expressed as follows:

$$g_{12} = \frac{1}{l_1^2l_2^2s_2^2}\Big\{g_{12}l_2^2\left(l_1^2 + 2l_1l_2c_2 + l_2^2\right) - g_{12}\left(l_2^2 + l_1l_2c_2\right)\left(l_2^2 + l_1l_2c_2\right)\Big\}. \tag{43}$$

By adding and subtracting $g_{11}l_2^2(l_2^2+l_1l_2c_2)$ inside the brace and then rearranging and combining the like terms, we have

$$g_{12}=\frac{1}{l_1^2l_2^2s_2^2}\left\{\bar{g}_{11}l_2^2+\bar{g}_{12}\left(l_2^2+l_1l_2c_2\right)\right\} \tag{44}$$

where $\bar{g}_{11}$ and $\bar{g}_{12}$ are, respectively, defined in (26) and (27). Substituting (34) and (41) into (44), we can finally transform g_{12} into the following form:

$$g_{12}=\frac{1}{l_1l_2s_2}\left\{\left(l_2^2+l_1l_2c_2\right)z_{p1}^C\left(u_{p2}-u_{p1}\right) -l_2^2z_{p0}^C\left(u_{p2}-u_{p0}\right)\right\}. \tag{45}$$

B. New Representations of g_{21} and g_{22}

Using the identity (23), we can express g_{21} as

$$g_{21}=\frac{1}{l_1^2l_2^2s_2^2}\left\{g_{21}l_2^2\left(l_1^2+2l_1l_2c_2+l_2^2\right) -g_{21}\left(l_2^2+l_1l_2c_2\right)\left(l_2^2+l_1l_2c_2\right)\right\} \tag{46}$$

which, by adding and subtracting $g_{22}(l_2^2+l_1l_2c_2)(l_1^2+2l_1l_2c_2+l_2^2)$, can be further rewritten as

$$g_{21}=\frac{1}{l_1^2l_2^2s_2^2}\left\{\bar{g}_{21}\left(l_2^2+l_1l_2c_2\right)+\bar{g}_{22}\left(l_1^2+2l_1l_2c_2+l_2^2\right)\right\} \tag{47}$$

where we have defined

$$\bar{g}_{21}=-g_{21}\left(l_2^2+l_1l_2c_2\right)+g_{22}\left(l_1^2+2l_1l_2c_2+l_2^2\right) \tag{48}$$

$$\bar{g}_{22}=g_{21}l_2^2-g_{22}\left(l_2^2+l_1l_2c_2\right). \tag{49}$$

Substituting (15) and (16) into (48), we can readily get

$$\bar{g}_{21}=h_{21}\Psi_1-h_{22}\Psi_2+v_{p2}(-h_{31}\Psi_1+h_{32}\Psi_2). \tag{50}$$

Further substituting (29) and (30) into (50), we can obtain

$$\bar{g}_{21}=-l_1l_2s_2\big\{h_{21}(l_1c_1+l_2c_{12})+h_{22}(l_1s_1+l_2s_{12}) -v_{p2}[h_{31}(l_1c_1+l_2c_{12})+h_{32}(l_1s_1+l_2s_{12})]\big\}. \tag{51}$$

From the definitions of $\boldsymbol{x}_{p2}$ and $\boldsymbol{x}_{p0}$, we can derive that

$$h_{21}(l_1c_1+l_2c_{12})+h_{22}(l_1s_1+l_2s_{12})=\boldsymbol{h}_2^\top\left\{\begin{bmatrix}\boldsymbol{x}_{p2}\\1\end{bmatrix}-\begin{bmatrix}\boldsymbol{x}_{p0}\\1\end{bmatrix}\right\} =z_{p2}^Cv_{p2}-z_{p0}^Cv_{p0} \tag{52}$$

where (8) and (22) have been used. Substituting (33) and (52) into (51) directly leads to

$$\bar{g}_{21}=-l_1l_2s_2z_{p0}^C(v_{p2}-v_{p0}). \tag{53}$$

Substituting (15) and (16) into (49), we have

$$\bar{g}_{22}=-h_{21}\Psi_3+h_{22}\Psi_4+v_{p2}(h_{31}\Psi_3-h_{32}\Psi_4). \tag{54}$$

Substituting (36) and (37) into (54) obtains

$$\bar{g}_{22}=l_1l_2s_2\big\{h_{21}(l_2c_{12})+h_{22}(l_2s_{12}) -v_{p2}[h_{31}(l_2c_{12})+h_{32}(l_2s_{12})]\big\}. \tag{55}$$

It is noted that

$$h_{21}(l_2c_{12})+h_{22}(l_2s_{12})=\boldsymbol{h}_2^\top\left\{\begin{bmatrix}\boldsymbol{x}_{p2}\\1\end{bmatrix}-\begin{bmatrix}\boldsymbol{x}_{p1}\\1\end{bmatrix}\right\} =z_{p2}^Cv_{p2}-z_{p1}^Cv_{p1} \tag{56}$$

where (8) and (19) are used. Then, substituting (40) and (56) into (55), it can be deduced that

$$\bar{g}_{22}=l_1l_2s_2z_{p1}^C(v_{p2}-v_{p1}). \tag{57}$$

Finally, substituting (53) and (57) into (47), we obtain

$$g_{21}=\frac{1}{l_1l_2s_2}\left\{(l_1^2+2l_1l_2c_2+l_2^2)z_{p1}^C(v_{p2}-v_{p1}) -(l_2^2+l_1l_2c_2)z_{p0}^C(v_{p2}-v_{p0})\right\}. \tag{58}$$

Now, it is time to derive the new representation of g_{22}.

With the help of (23), g_{22} can be transformed to

$$g_{22}=\frac{1}{l_1^2l_2^2s_2^2}\left\{g_{22}l_2^2\left(l_1^2+2l_1l_2c_2+l_2^2\right) -g_{22}\left(l_2^2+l_1l_2c_2\right)\left(l_2^2+l_1l_2c_2\right)\right\}. \tag{59}$$

By adding and subtracting $g_{21}l_2^2(l_2^2+l_1l_2c_2)$ inside the brace, it can be demonstrated that

$$g_{22}=\frac{1}{l_1^2l_2^2s_2^2}\left\{\bar{g}_{21}l_2^2+\bar{g}_{22}\left(l_2^2+l_1l_2c_2\right)\right\} \tag{60}$$

where $\bar{g}_{21}$ and $\bar{g}_{22}$ are, respectively, given in (48) and (49). From (53) and (57), it can be easily derived that

$$g_{22}=\frac{1}{l_1l_2s_2}\left\{\left(l_2^2+l_1l_2c_2\right)z_{p1}^C\left(v_{p2}-v_{p1}\right)-l_2^2z_{p0}^C\left(v_{p2}-v_{p0}\right)\right\}. \tag{61}$$

Up to now, we have developed the new image-space kinematic model of the 2DOFs planar manipulator as follows:

$$\dot{\boldsymbol{y}}_{p2}=\frac{1}{z_{p2}^C}\mathbf{G}_{p2}\begin{bmatrix}\dot{\theta}_1\\\dot{\theta}_2\end{bmatrix}\triangleq\mathbf{J}_i\begin{bmatrix}\dot{\theta}_1\\\dot{\theta}_2\end{bmatrix} \tag{62}$$

where $\mathbf{J}_i\in\Re^{2\times2}$ denotes the image Jacobian of 2DOFs planar manipulators and can be expressed in the following form:

$$\mathbf{J}_i=\frac{1}{l_1l_2s_2}\frac{1}{z_{p2}^C}\begin{bmatrix}z_{p0}^C\left(u_{p2}-u_{p0}\right) & z_{p1}^C\left(u_{p2}-u_{p1}\right)\\ z_{p0}^C\left(v_{p2}-v_{p0}\right) & z_{p1}^C\left(v_{p2}-v_{p1}\right)\end{bmatrix} \times\begin{bmatrix}-\left(l_2^2+l_1l_2c_2\right) & -l_2^2\\ l_1^2+2l_1l_2c_2+l_2^2 & l_2^2+l_1l_2c_2\end{bmatrix}. \tag{63}$$

From (63), it is clear that the new image-space kinematic model is completely independent of the camera parameters, which meets the requirement for the design of fully uncalibrated image-based controllers.

IV. Proposed Image-Based Controllers

We will develop two new fully uncalibrated image-based controllers, respectively, for two different cases: 1) the parallel case where the camera is installed such that the robot motion plane and the image plane are parallel, and 2) the general case where the camera is fixed at an arbitrary pose without the parallelism requirement.

A. Controller Design for the Parallel Case

We can know that the depths of the feature points are constant in the parallel case, and they are always equal. Hence, we have $z_{p0}^C \equiv z_{p1}^C \equiv z_{p2}^C$. Based on this relationship, the new image-space kinematics (62) can be simplified as

$$\dot{\boldsymbol{y}}_{p2} = \mathbf{J}_{ip}\begin{bmatrix}\dot{\theta}_1\\ \dot{\theta}_2\end{bmatrix} \tag{64}$$

where $\mathbf{J}_{ip}$ denotes the image Jacobian of 2DOFs planar manipulators in the parallel case

$$\mathbf{J}_{ip} = \frac{1}{l_1 l_2 s_2}\begin{bmatrix}u_{p2}-u_{p0} & u_{p2}-u_{p1}\\ v_{p2}-v_{p0} & v_{p2}-v_{p1}\end{bmatrix} \times \begin{bmatrix}-(l_2^2+l_1l_2c_2) & -l_2^2\\ l_1^2+2l_1l_2c_2+l_2^2 & l_2^2+l_1l_2c_2\end{bmatrix} \tag{65}$$

and it is called the depth-free image Jacobian.

From (65), we can clearly see that the derived new image-space kinematic model has nice properties, that is, without depending on the camera parameters and the feature depths. Hence, calibration/estimation and compensation of the unknown feature depths and camera parameters, which are necessary in traditional IBVS controllers, can be avoided when the new kinematic model (64) is used for controller development. This can simplify the controller design and provide a good way to achieve high-performance visual servoing systems in the face of camera parameter uncertainties.

Proposition 1: The depth-free image Jacobian $\mathbf{J}_{ip}$ is always nonsingular.

Proof: The determinant of $\mathbf{J}_{ip}$ can be calculated as

$$\det \mathbf{J}_{ip} = \det\big[\boldsymbol{y}_{p2}-\boldsymbol{y}_{p0}\ \boldsymbol{y}_{p2}-\boldsymbol{y}_{p1}\big]. \tag{66}$$

Under the nonsingularity assumption of the analytical Jacobian, we have $s_2 \neq 0$, which means that $\mathbf{J}_{ip}$ is well defined and directly implies that the feature points P_2, P_1, and P_0 will not lie on the same straight line in the motion plane. This means that the image coordinates $\boldsymbol{y}_{p2}, \boldsymbol{y}_{p1}$, and $\boldsymbol{y}_{p0}$ of the feature points will not be collinear in the image plane under the perspective projection assumption, except when the camera is placed in the motion plane, which is impossible in practical applications. In this regard, we know that $\det[\boldsymbol{y}_{p2}-\boldsymbol{y}_{p0}\ \boldsymbol{y}_{p2}-\boldsymbol{y}_{p1}]$ is nonzero. Hence, we conclude that $\det \mathbf{J}_{ip} \neq 0$, and $\mathbf{J}_{ip}$ is nonsingular. ■

Due to the nonsingularity of $\mathbf{J}_{ip}$, we can use its inverse to design the following velocity controller for the 2DOFs planar manipulator:

$$\begin{bmatrix}\dot{\theta}_1\\ \dot{\theta}_2\end{bmatrix} = -\mathbf{J}_{ip}^{-1}\mathbf{K}_{ip}\Delta\boldsymbol{y}_{p2} \tag{67}$$

where $\mathbf{K}_{ip} \in \Re^{2\times 2}$ denotes a symmetric positive-definite matrix. Now, the result for the parallel case is stated as follows.

Theorem 1: In the case where the motion and image planes are parallel, by applying the controller (67), the feature point P_2 is regulated to its desired image position at an exponential rate, that is, $\Delta\boldsymbol{y}_{p2} \to \mathbf{0}$ exponentially as $t \to \infty$.

Proof: Substituting (67) into the image-space kinematics (64) directly leads to the closed-loop system

$$\Delta\dot{\boldsymbol{y}}_{p2} = -\mathbf{K}_{ip}\Delta\boldsymbol{y}_{p2} \tag{68}$$

where we have used the fact that $\Delta\dot{\boldsymbol{y}}_{p2} = \dot{\boldsymbol{y}}_{p2} - \dot{\boldsymbol{y}}_{p2}^d = \dot{\boldsymbol{y}}_{p2}$ since for a constant desired image position, we have $\dot{\boldsymbol{y}}_{p2}^d = \mathbf{0}$. Based on (68), it can be concluded that $\Delta\boldsymbol{y}_{p2}$ will exponentially converge to zero as $t \to \infty$. ■

Remark 1: In the case where there exists kinematic uncertainty, only an estimate of the Jacobian matrix can be obtained, and the controller should be modified by designing adaptive laws. Note that $\mathbf{J}_{ip}$ can be rewritten as

$$\mathbf{J}_{ip} = \frac{1}{s_2}\begin{bmatrix}\delta_{20}^u & \delta_{21}^u\\ \delta_{20}^v & \delta_{21}^v\end{bmatrix}\begin{bmatrix}-(\rho_{l2}+c_2) & -\rho_{l2}\\ \rho_{l1}+2c_2+\rho_{l2} & \rho_{l2}+c_2\end{bmatrix}$$

where $\delta_{ij}^u = u_{pi}-u_{pj}$, $\delta_{ij}^v = v_{pi}-v_{pj}$, $i,j = 0,1,2$, $\rho_{l1} = \frac{l_1}{l_2}$, and $\rho_{l2} = \frac{l_2}{l_1}$. Here, we can see that uncertainties in the length ratios $\boldsymbol{\rho}_l = (\rho_{l1}, \rho_{l2})^\top$, but not in the lengths, can affect the control performance of the 2DOFs planar manipulator. Hence, in this case, adaptive laws should be developed to deal with the length ratio uncertainties. Denote the estimate of the length ratios by $\hat{\boldsymbol{\rho}}_l = (\hat{\rho}_{l1}, \hat{\rho}_{l2})^\top$. Then, we can analytically calculate the estimated inverse Jacobian $\hat{\mathbf{J}}_{ip}^{-1}$ as

$$\hat{\mathbf{J}}_{ip}^{-1} = \frac{1}{\chi_1 s_2}\begin{bmatrix}\chi_3 & \hat{\rho}_{l2}\\ -(\chi_2+\chi_3) & -\chi_3\end{bmatrix}\begin{bmatrix}\delta_{21}^v & -\delta_{21}^u\\ -\delta_{20}^v & \delta_{20}^u\end{bmatrix}$$

where $\chi_1 = \det[\boldsymbol{y}_{p2}-\boldsymbol{y}_{p0}\ \boldsymbol{y}_{p2}-\boldsymbol{y}_{p1}]$, $\chi_2 = \hat{\rho}_{l1}+c_2$, and $\chi_3 = \hat{\rho}_{l2}+c_2$. Note that $\hat{\mathbf{J}}_{ip}^{-1}$ is obtained from the analytical expression of the inverse Jacobian $\mathbf{J}_{ip}^{-1}$ by replacing the length ratios $\boldsymbol{\rho}_l$ with the estimated values $\hat{\boldsymbol{\rho}}_l$. In this way, the singularity issue arising from the parameter estimation, which exists in traditional approaches that compute the estimated inverse Jacobian via numerical inversion of the estimated Jacobian $\hat{\mathbf{J}}_{ip}$, can be avoided. In the presence of kinematic uncertainty, the controller (67) can be modified as

$$\begin{bmatrix}\dot{\theta}_1\\ \dot{\theta}_2\end{bmatrix} = -\chi_4\hat{\mathbf{J}}_{ip}^{-1}\mathbf{K}_{ip}\Delta\boldsymbol{y}_{p2}$$

where $\chi_4 = 1/s_2^2(\hat{\rho}_{l1}\hat{\rho}_{l2}-c_2^2)$. Accordingly, the adaptive law should be designed to update the estimated length ratios $\hat{\boldsymbol{\rho}}_l$ as

$$\dot{\hat{\boldsymbol{\rho}}}_l = \frac{\chi_4}{\chi_1 s_2^2}\Gamma_l^{-1}\begin{bmatrix}-\varepsilon_{21}^{uv} & 0\\ \varepsilon_{10}^{uv} & \varepsilon_{10}^{uv}\end{bmatrix}\begin{bmatrix}\chi_3 & \hat{\rho}_{l2}\\ -(\chi_2+\chi_3) & -\chi_3\end{bmatrix} \times \begin{bmatrix}\delta_{21}^v & -\delta_{21}^u\\ -\delta_{20}^v & \delta_{20}^u\end{bmatrix}\mathbf{K}_{ip}\Delta\boldsymbol{y}_{p2}$$

where $\Gamma_l \in \Re^{2\times 2}$ is a symmetric positive-definite matrix, $\varepsilon_{10}^{uv} = \Delta u_{p2}\delta_{10}^u + \Delta v_{p2}\delta_{10}^v$, and $\varepsilon_{21}^{uv} = \Delta u_{p2}\delta_{21}^u + \Delta v_{p2}\delta_{21}^v$. Using Lyapunov stability theory, it can be shown that the modified controller and the designed adaptive law can guarantee asymptotical convergence of the image position error $\Delta\boldsymbol{y}_{p2}$ in the presence of kinematic uncertainty.

B. Controller Design for the General Case

In the case where the camera is fixed at a general pose, the new kinematics (62) can be rewritten as

$$\dot{\boldsymbol{y}}_{p2} = \mathbf{J}_{ig}\begin{bmatrix}\dot{\theta}_1\\ \dot{\theta}_2\end{bmatrix} \tag{69}$$

where $\mathbf{J}_{ig}$ denotes the image Jacobian of the planar manipulator in the general case

$$\mathbf{J}_{ig} = \frac{1}{l_1 l_2 s_2}\begin{bmatrix} \alpha_{02}(u_{p2}-u_{p0}) & \alpha_{12}(u_{p2}-u_{p1}) \\ \alpha_{02}(v_{p2}-v_{p0}) & \alpha_{12}(v_{p2}-v_{p1}) \end{bmatrix} \times \begin{bmatrix} -(l_2^2+l_1 l_2 c_2) & -l_2^2 \\ l_1^2+2l_1 l_2 c_2+l_2^2 & l_2^2+l_1 l_2 c_2 \end{bmatrix}. \quad (70)$$

Here, $\alpha_{02} = z_{p0}^C/z_{p2}^C$ and $\alpha_{12} = z_{p1}^C/z_{p2}^C$ are depth ratios between the points P_0, P_1, and P_2, and $\mathbf{J}_{ig}$ is called the depth-ratio-based image Jacobian.

One main difficulty of the controller design using traditional image-space kinematic models is that without using other sensors, we cannot directly measure/compute the feature depths based on images of a single camera. This difficulty can be avoided when the proposed image-space kinematics is used for controller design. It is noted that different from the depth information, the depth ratios in the proposed kinematic model can be estimated from motion information of the planar manipulator and image information of the feature points, as stated in the following proposition.

Proposition 2: When the manipulator motion satisfies the conditions

$$\begin{aligned} \left(l_2^2+l_1 l_2 c_2\right)\dot{\theta}_1 + l_2^2\dot{\theta}_2 \neq 0 \\ \left(l_1^2+2l_1 l_2 c_2+l_2^2\right)\dot{\theta}_1 + \left(l_2^2+l_1 l_2 c_2\right)\dot{\theta}_2 \neq 0 \end{aligned} \quad (71)$$

the depth ratios α_{02} and α_{12} can be obtained as

$$\begin{bmatrix} \alpha_{02} \\ \alpha_{12} \end{bmatrix} = \mathbf{W}_{i\alpha}^{-1}\dot{\boldsymbol{y}}_{p2} \quad (72)$$

where $\dot{\boldsymbol{y}}_{p2}$ is the optical flow of P_2, $\mathbf{W}_{i\alpha}$ is defined as

$$\mathbf{W}_{i\alpha} = \begin{bmatrix} \dot{\theta}_{i1}(u_{p2}-u_{p0}) & \dot{\theta}_{i2}(u_{p2}-u_{p1}) \\ \dot{\theta}_{i1}(v_{p2}-v_{p0}) & \dot{\theta}_{i2}(v_{p2}-v_{p1}) \end{bmatrix}$$

and $\dot{\theta}_{i1}$ and $\dot{\theta}_{i2}$ are given by

$$\begin{bmatrix} \dot{\theta}_{i1} \\ \dot{\theta}_{i2} \end{bmatrix} = \frac{1}{l_1 l_2 s_2}\begin{bmatrix} -(l_2^2+l_1 l_2 c_2) & -l_2^2 \\ l_1^2+2l_1 l_2 c_2+l_2^2 & l_2^2+l_1 l_2 c_2 \end{bmatrix}\begin{bmatrix} \dot{\theta}_1 \\ \dot{\theta}_2 \end{bmatrix}. \quad (73)$$

Proof: Based on (73), (69) can be rewritten as

$$\dot{\boldsymbol{y}}_{p2} = \begin{bmatrix} \alpha_{02}(u_{p2}-u_{p0}) & \alpha_{12}(u_{p2}-u_{p1}) \\ \alpha_{02}(v_{p2}-v_{p0}) & \alpha_{12}(v_{p2}-v_{p1}) \end{bmatrix}\begin{bmatrix} \dot{\theta}_{i1} \\ \dot{\theta}_{i2} \end{bmatrix}$$

which can be further transformed in the following form:

$$\dot{\boldsymbol{y}}_{p2} = \mathbf{W}_{i\alpha}\begin{bmatrix} \alpha_{02} \\ \alpha_{12} \end{bmatrix}. \quad (74)$$

The determinant of $\mathbf{W}_{i\alpha}$ can be obtained as follows:

$$\det \mathbf{W}_{i\alpha} = \dot{\theta}_{i1}\dot{\theta}_{i2}\det\left[\boldsymbol{y}_{p2}-\boldsymbol{y}_{p0}\ \boldsymbol{y}_{p2}-\boldsymbol{y}_{p1}\right].$$

From the proof of Proposition 1, we can know that $\det[\boldsymbol{y}_{p2}-\boldsymbol{y}_{p0}\ \boldsymbol{y}_{p2}-\boldsymbol{y}_{p1}] \neq 0$ under the nonsingularity assumption of the analytical Jacobian matrix. If the conditions in (71) are satisfied by the robot motion, according to (73) we have $\dot{\theta}_{i1} \neq 0$ and $\dot{\theta}_{i2} \neq 0$, which implies that $\det \mathbf{W}_{i\alpha} \neq 0$. Hence, from (74) and using the optical flow technique, the depth ratios α_{02} and α_{12} can be computed by (72). ■

Once the depth ratios α_{02} and α_{12} are measured, the depth-ratio-based image Jacobian $\mathbf{J}_{ig}$ can be obtained from joint position information of the manipulator and image information of the feature points, with no knowledge about the camera parameters. Then, if the depth-ratio-based image Jacobian is nonsingular, its inverse can be directly used for designing the velocity controller.

Proposition 3: The depth-ratio-based image Jacobian $\mathbf{J}_{ig}$ is always nonsingular.

Proof: The determinant of $\mathbf{J}_{ig}$ is given by

$$\det \mathbf{J}_{ig} = \alpha_{02}\alpha_{12}\det\left[\boldsymbol{y}_{p2}-\boldsymbol{y}_{p0}\ \boldsymbol{y}_{p2}-\boldsymbol{y}_{p1}\right]. \quad (75)$$

From the proof of Proposition 2, we know that $s_2 \neq 0$ and $\det[\boldsymbol{y}_{p2}-\boldsymbol{y}_{p0}\ \boldsymbol{y}_{p2}-\boldsymbol{y}_{p1}] \neq 0$ under the nonsingularity assumption of the analytical Jacobian matrix. Since α_{02} and α_{12} are always positive, we have $\det \mathbf{J}_{ig} \neq 0$ based on (75). Hence, $\mathbf{J}_{ig}$ is well defined and always nonsingular. ■

Now, the velocity controller for the general case can be designed as follows:

$$\begin{bmatrix} \dot{\theta}_1 \\ \dot{\theta}_2 \end{bmatrix} = -\mathbf{J}_{ig}^{-1}\mathbf{K}_{ig}\Delta\boldsymbol{y}_{p2} \quad (76)$$

where $\mathbf{K}_{ig} \in \Re^{2\times 2}$ denotes a symmetric positive-definite matrix. Now, we have the following result for the general case.

Theorem 2: In the case where the camera is mounted at a general pose, by applying the velocity controller (76), the feature point P_2 is regulated to its desired image position at an exponential rate, that is, $\Delta\boldsymbol{y}_{p2} \to \mathbf{0}$ exponentially as $t \to \infty$.

Proof: Substituting (76) into the image-space kinematic model (69) results in

$$\Delta\dot{\boldsymbol{y}}_{p2} = -\mathbf{K}_{ig}\Delta\boldsymbol{y}_{p2} \quad (77)$$

which implies the exponential convergence of $\Delta\boldsymbol{y}_{p2}$ and directly proves the result. ■

Remark 2: When there exist kinematic uncertainties in the general case, it is necessary to design proper algorithms to simultaneously estimate the unknown depth ratios (α_{02}, α_{12}) and the uncertain length ratios $\boldsymbol{\rho}_l$. This is very difficult, if not impossible, without suitable assumptions. To circumvent this difficulty, it is assumed that the depth ratios are constant or slowly time varying, which makes it possible to develop updating laws for the online estimation of the coupled parameters $\boldsymbol{\rho}_{l\alpha} = (\rho_{l\alpha 1}, \rho_{l\alpha 2}, \ldots, \rho_{l\alpha 5})^\top \triangleq (1/\alpha_{02}, 1/\alpha_{12}, \rho_{l1}/\alpha_{02}, \rho_{l2}/\alpha_{02}, \rho_{l2}/\alpha_{12})^\top$ involved in the Jacobian $\mathbf{J}_{ig}$. Denoting the estimated coupled parameters by $\hat{\boldsymbol{\rho}}_{l\alpha} = (\hat{\rho}_{l\alpha 1}, \hat{\rho}_{l\alpha 2}, \ldots, \hat{\rho}_{l\alpha 5})^\top$. To avoid the singularity issue arised from parameter estimation, as done in *Remark 1*, the following estimated inverse Jacobian $\hat{\mathbf{J}}_{ig}^{-1}$, which is obtained from the analytical inverse Jacobian $\mathbf{J}_{ig}^{-1}$ by replacing the unknown coupled parameters $\boldsymbol{\rho}_{l\alpha}$ by the estimated values $\hat{\boldsymbol{\rho}}_{l\alpha}$, is used for controller design

$$\hat{\mathbf{J}}_{ig}^{-1} = \frac{1}{\chi_1 s_2}\begin{bmatrix} \chi_5\delta_{21}^v - \hat{\rho}_{l\alpha 5}\delta_{20}^v & \hat{\rho}_{l\alpha 5}\delta_{20}^u - \chi_5\delta_{21}^u \\ \chi_7\delta_{20}^v - \chi_8\delta_{21}^v & \chi_8\delta_{21}^u - \chi_7\delta_{20}^u \end{bmatrix}$$

where $\chi_5 = c_2\hat{\rho}_{l\alpha 1} + \hat{\rho}_{l\alpha 4}$, $\chi_6 = c_2\hat{\rho}_{l\alpha 1} + \hat{\rho}_{l\alpha 3}$, $\chi_7 = c_2\hat{\rho}_{l\alpha 2} + \hat{\rho}_{l\alpha 5}$, and $\chi_8 = \chi_5 + \chi_6$. Now, the controller for the general case in the presence of kinematic uncertainty is designed as

$$\begin{bmatrix} \dot{\theta}_1 \\ \dot{\theta}_2 \end{bmatrix} = -\tanh(\chi_9)\hat{\mathbf{J}}_{ig}^{-1}\mathbf{K}_{ig}\Delta\boldsymbol{y}_{p2}$$

where $\chi_9 = 1/s_2^2\{\hat{\rho}_{l\alpha 3}\hat{\rho}_{l\alpha 5} + (\hat{\rho}_{l\alpha 1}\hat{\rho}_{l\alpha 5} - \hat{\rho}_{l\alpha 2}\hat{\rho}_{l\alpha 4})c_2 - \hat{\rho}_{l\alpha 1}\hat{\rho}_{l\alpha 2}c_2^2\}$. Accordingly, the adaptive law should be designed as

$$\dot{\hat{\boldsymbol{\rho}}}_{l\alpha} = \frac{\tanh(\chi_9)}{\chi_1 s_2^2}\Gamma_{l\alpha}^{-1} \times \begin{bmatrix} -2c_2\varepsilon_{21}^{uv} & c_2\varepsilon_{20}^{uv} & -\varepsilon_{21}^{uv} & -\varepsilon_{21}^{uv} & \varepsilon_{20}^{uv} \\ -c_2\varepsilon_{21}^{uv} & 0 & 0 & -\varepsilon_{21}^{uv} & \varepsilon_{20}^{uv} \end{bmatrix}^\top \times \begin{bmatrix} \chi_5\delta_{21}^v - \hat{\rho}_{l\alpha 5}\delta_{20}^v & \hat{\rho}_{l\alpha 5}\delta_{20}^u - \chi_5\delta_{21}^u \\ \chi_7\delta_{20}^v - \chi_8\delta_{21}^v & \chi_8\delta_{21}^u - \chi_7\delta_{20}^u \end{bmatrix}\mathbf{K}_{ig}\Delta\boldsymbol{y}_{p2}$$

where $\Gamma_{l\alpha} \in \Re^{5\times 5}$ is a symmetric positive-definite matrix, and $\varepsilon_{20}^{uv} = \Delta u_{p2}\delta_{20}^u + \Delta v_{p2}\delta_{20}^v$. Then, based on the Lyapunov stability theory, it can be shown that in the presence of kinematic uncertainty, asymptotical convergence of $\Delta\boldsymbol{y}_{p2}$ is guaranteed by the adaptive controller proposed here.

Remark 3: In the developed approaches, only kinematics is considered without taking into account the manipulator dynamics. In the kinematics-based controller design, it is assumed that via the use of low-level controllers in the robot platforms, velocity commands can be perfectly tracked by the actual velocity instantaneously. In real environments, however, such a perfect velocity tracking assumption does not hold generally, and so the control performance can be affected in real applications when only kinematics is considered in the controller design. Hence, to obtain higher control performance in real environments, the manipulator dynamics should be considered in the controller design, especially when the torque commands can be received by the robot platforms. In this regard, the developed approaches can be extended to deal with the manipulator dynamics by adding the velocity damping and gravity compensation terms [51].

Remark 4: The developed approaches can only handle the position regulation control problem and cannot be used for tracking of a desired trajectory in the image space. To deal with the trajectory tracking control problem, the developed controllers can be modified by adding a desired image velocity-based feedforward compensation term as

$$\begin{bmatrix} \dot{\theta}_1 \\ \dot{\theta}_2 \end{bmatrix} = \mathbf{J}^{-1}\left(\dot{\boldsymbol{y}}_{p2}^d - \mathbf{K}\Delta\boldsymbol{y}_{p2}\right)$$

where the image Jacobian $\mathbf{J}$ and the gain matrix $\mathbf{K}$, respectively, denote $\mathbf{J}_{ip}$ and $\mathbf{K}_{ip}$ in the parallel case, or $\mathbf{J}_{ig}$ and $\mathbf{K}_{ig}$ in the general case, and $\dot{\boldsymbol{y}}_{p2}^d$ is the time-varying image velocity corresponding to the desired trajectory in the image space.

V. Simulation Results

Simulation results are provided in this section to show the effectiveness of the developed fully uncalibrated IBVS approaches. We assume that the homogeneous transformation matrix between the coordinate frames B and C can be determined via a series of basic transformations in the way

$$\mathbf{T}_C^B = \mathrm{R}(\boldsymbol{x}, \pi - \phi_1)\mathrm{R}(\boldsymbol{y}, \phi_2)\mathrm{R}(\boldsymbol{z}, \phi_3)\mathrm{T}(a_1, a_2, -a_3)$$

where $\mathrm{R}(\boldsymbol{\zeta}, \vartheta)$ ($\boldsymbol{\zeta} = \boldsymbol{x}, \boldsymbol{y}, \boldsymbol{z}$ and $\vartheta = \pi - \phi_1, \phi_2, \phi_3$, respectively) is a rotational transformation about $\boldsymbol{\zeta}$-axis by ϑ, $\mathrm{T}(a_1, a_2, -a_3)$ denotes a translational transformation

$$\mathrm{T}(a_1, a_2, -a_3) = \begin{bmatrix} \mathbf{I}_{3\times 3} & (a_1, a_2, -a_3)^\top \\ \mathbf{0}_{1\times 3} & 1 \end{bmatrix}$$

and ϕ_1, ϕ_2, ϕ_3, a_1, a_2, and a_3 are scalar constants to define a specific camera setup. The camera extrinsic matrix can be obtained by inverting the matrix $\mathbf{T}_C^B$, that is, $\mathbf{T}_B^C = \{\mathbf{T}_C^B\}^{-1}$.

In the simulations, for the parallel case, the parameters ϕ_1, ϕ_2, ϕ_3, a_1, a_2 and a_3 are assumed to be $\phi_1 = \phi_2 = \phi_3 = 0$ rad, $a_1 = a_2 = 1$ m and $a_3 = 3$ m. For the general case, we set $\phi_1 = \pi/3$ rad while keeping other parameters unchanged. The camera intrinsic parameters are given by $k_v = k_u = 1800$ pixels/m, $v_0 = 250$ pixels, $u_0 = 280$ pixels, and $f = 0.035$ m. The camera intrinsic matrix $\mathbf{A}$ can be obtained as

$$\mathbf{A} = \begin{bmatrix} fk_u & 0 & u_0 \\ 0 & fk_v & v_0 \\ 0 & 0 & 1 \end{bmatrix}.$$

Note that neither online nor offline camera calibration is required for the controller design, and no priori information about the camera parameters is needed.

Furthermore, the lengths of the first and second links of the 2DOFs planar manipulator are set to $l_1 = l_2 = 1$ m, and the initial joint position is assumed to be $\boldsymbol{\theta}(0) = (\theta_1(0), \theta_2(0))^\top = (0, \pi/12)^\top$ rad. The desired image position $\boldsymbol{y}_{p2}^d$ of P_2 can be obtained via the teach-by-showing approach, that is, the image position of P_2 extracted from a desired image, which is captured when the manipulator is manually moved to a desired joint position $\boldsymbol{\theta}^d$ or Cartesian position $\boldsymbol{x}_{p2}^d$, is taken as the desired image position $\boldsymbol{y}_{p2}^d$. For all simulations, the desired joint position is set to $\boldsymbol{\theta}^d = (\pi/6, \pi/3)^\top$ rad, which corresponds to the desired Cartesian position $\boldsymbol{x}_{p2}^d = (0.866, 1.5)^\top$ m.

Under the above settings, the objective of the simulations is to use image information from a fully uncalibrated fixed camera to control the manipulator motion such that the feature point P_2 can arrive at the desired image position $\boldsymbol{y}_{p2}^d = (277.1865, 197.5)^\top$ pixels for the parallel case and $\boldsymbol{y}_{p2}^d = (275.0379, 185.1837)^\top$ pixels for the general case. For the parallel case, simulation results corresponding to the controller (67) with the gain $\mathbf{K}_{ip} = 0.5\mathbf{I}_{2\times 2}$ are presented in Fig. 3. From Fig. 3, it can be seen that the image position error $\Delta\boldsymbol{y}_{p2}$ is guaranteed to converge to zero, which validates the conclusion in Theorem 1. Furthermore, the motion plane trajectory and position errors of P_2 are also given in Fig. 4, which shows that the feature point P_2 can be guaranteed to equivalently reach the desired Cartesian-space position. The joint position errors and control inputs are provided in Fig. 5. For the general case, simulation results corresponding to the controller (76) with the gain $\mathbf{K}_{ig} = 0.5\mathbf{I}_{2\times 2}$ are shown in Figs. 6–8, which demonstrate the convergence of position errors and confirm the conclusion in Theorem 2. Hence, the proposed controllers can be used to efficiently handle the vision-based position control problem of 2DOFs planar manipulators without online or offline camera calibration.

VI. Experimental Results

In this section, experimental results based on the KUKA LBR iiwa 7DOFs robotic manipulator are provided to further show the effectiveness of the developed fully uncalibrated IBVS approaches. In the experiments, only 2DOFs (the second

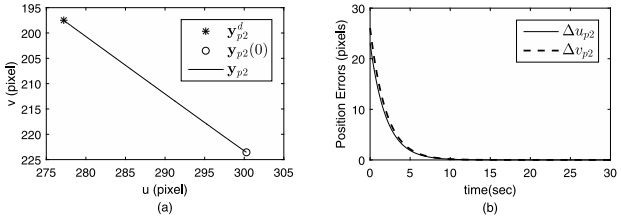

Fig. 3. Simulation results for the controller (67): image plane trajectory and position errors of P_2. (a) Trajectory. (b) Position errors.

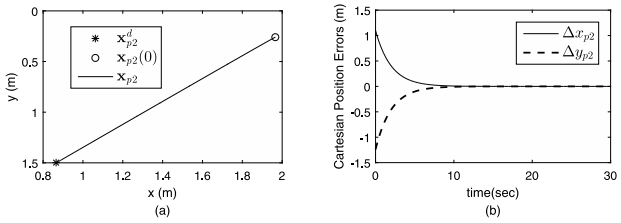

Fig. 4. Simulation results for the controller (67): motion plane trajectory and position errors of P_2. (a) Trajectory. (b) Position errors.

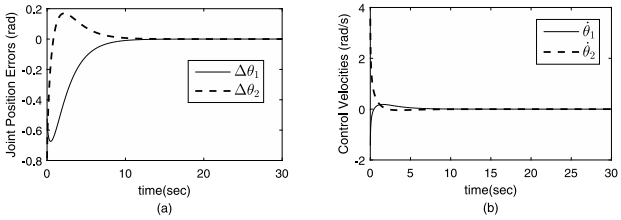

Fig. 5. Simulation results for the controller (67): joint position errors and control inputs. (a) Joint position errors. (b) Control inputs.

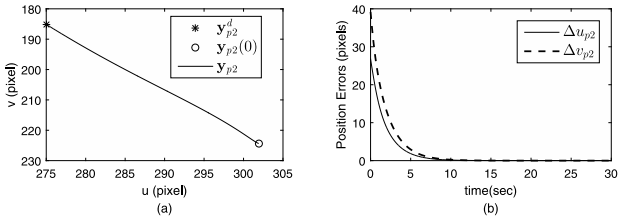

Fig. 6. Simulation results for the controller (76): image plane trajectory and position errors of P_2. (a) Trajectory. (b) Position errors.

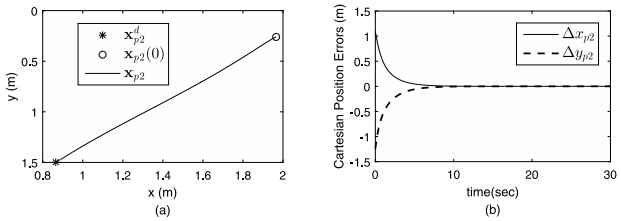

Fig. 7. Simulation results for the controller (76): motion plane trajectory and position errors of P_2. (a) Trajectory. (b) Position errors.

and fourth joints) of the robotic manipulator are used to constitute a 2DOFs planar manipulator, while keeping other DOFs fixed. The experimental system setup is shown in Fig. 9. To achieve a robust feature tracking, three colored (yellow, green and red) circular markers haven been, respectively, attached on the second, fourth, and sixth joints of the robotic manipulator, and their geometric centers are adopted to denote the

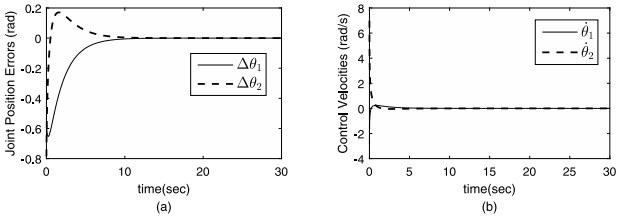

Fig. 8. Simulation results for the controller (76): joint position errors and control inputs. (a) Joint position errors. (b) Control inputs.

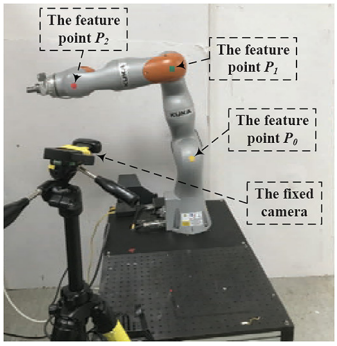

Fig. 9. Experimental system setup.

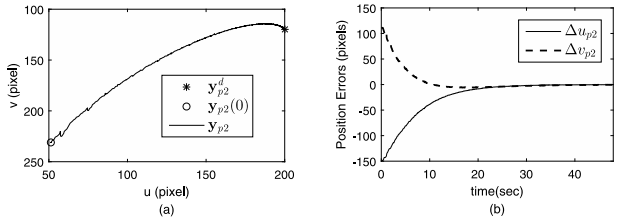

Fig. 10. Experimental results for the controller (67): image plane trajectory and position errors of P_2. (a) Trajectory. (b) Position errors.

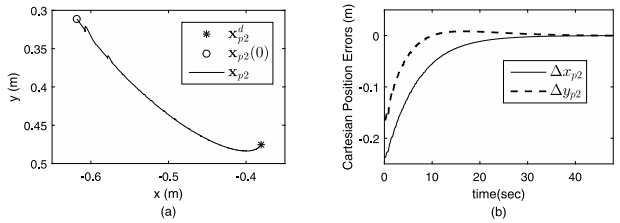

Fig. 11. Experimental results for the controller (67): motion plane trajectory and position errors of P_2. (a) Trajectory. (b) Position errors.

feature points P_0, P_1, and P_2, respectively, as shown in Fig. 9. Under this setting, the lengths of two links of such a 2DOFs planar manipulator are approximately equal and about 0.4 m. In the experiments, a Logitech USB camera is used to observe the motion of the feature points. The image processing algorithm and the developed controllers are both implemented on a work station with Intel Core i7-3610QM CPU and 7.7-GB RAM. The sampling time of the closed-loop system is about 40 ms. In the controller implementation, no knowledge about the camera intrinsic and extrinsic parameters is used.

In the experiments, the desired image position is set to be $\boldsymbol{y}_{p2}^d = (200, 120)^\top$ pixels for both the parallel and the general cases. Accordingly, the desired joint and Cartesian

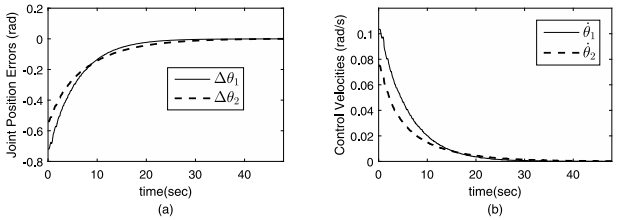

Fig. 12. Experimental results for the controller (67): joint position errors and control inputs. (a) Joint position errors. (b) Control inputs.

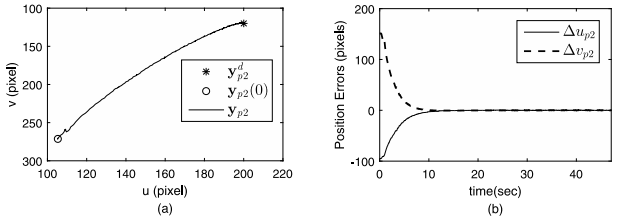

Fig. 13. Experimental results for the controller (76): image plane trajectory and position errors of P_2. (a) Trajectory. (b) Position errors.

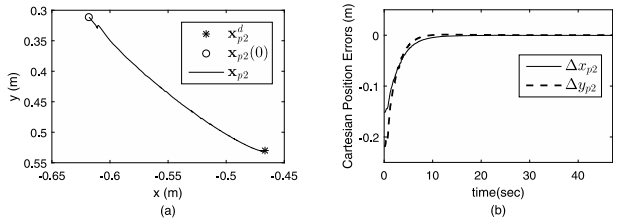

Fig. 14. Experimental results for the controller (76): motion plane trajectory and position errors of P_2. (a) Trajectory. (b) Position errors.

positions in the parallel case are, respectively, given by $\boldsymbol{\theta}^d = (0.0064, 1.8680)^\top$ rad and $\boldsymbol{x}_{p2}^d = (-0.3806, 0.4753)^\top$ m. While in the general case, the corresponding desired joint and Cartesian positions are, respectively, given by $\boldsymbol{\theta}^d = (-0.1762, 1.53)^\top$ rad and $\boldsymbol{x}_{p2}^d = (-0.4665, 0.5298)^\top$ m. The desired joint and Cartesian position information is used only for the experimental analysis but not for the controller design. For the parallel case, experimental results corresponding to the controller (67) with the controller gain $\mathbf{K}_{ip} = 0.007 \times \text{diag}(20, 13)$ are given in Figs. 10–12. From Figs. 10–12, we can clearly see that under the control of the developed controller (67), the image, Cartesian, and joint position errors all can be guaranteed to be convergent to zero, and the feature point P_2 can be ensured to arrive at the desired position in both the image and the Cartesian spaces, which confirms the conclusion in Theorem 1. For the general case, experimental results corresponding to the controller (76) with the controller gain $\mathbf{K}_{ig} = 0.007 \times \text{diag}(20, 13)$ are presented in Figs. 13–15, which also show the convergence of the image, Cartesian, and joint position errors and hence confirm the conclusion in Theorem 2. Based on the experimental results in Figs. 10–15, we know that the developed fully uncalibrated IBVS approaches can be applied in real applications to achieve a good position control performance of 2DOFs planar manipulators, though without using any knowledge about the fixed camera.

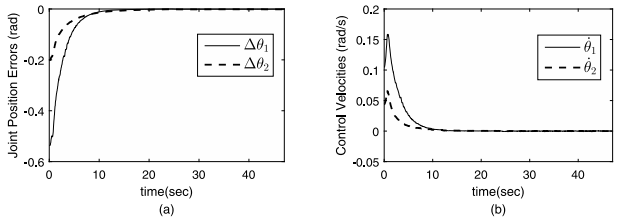

Fig. 15. Experimental results for the controller (76): joint position errors and control inputs. (a) Joint position errors. (b) Control inputs.

VII. Conclusion

In this work, we develop two novel controllers to address the fully uncalibrated visual servoing problem of 2DOFs planar manipulators with a fixed camera. The developed controllers are designed, respectively, using the depth-free and depth-ratio-based image Jacobian matrices, and can be implemented without depending on any *a priori* knowledge of the camera parameters. Different from traditional uncalibrated visual servoing controllers, the developed controllers do not require using numerical algorithms or adaptive laws for offline/online camera calibration and can make the control system design easier in real applications. Furthermore, due to the absence of parameter estimation, exponential convergence of image position errors is theoretically ensured. This makes it possible to design high-performance visual servoing systems for 2DOFs planar manipulators. Simulation and experimental results are given to show the effectiveness of the developed controllers. Note that the fully uncalibrated visual servoing problem is considered only for the case of 2DOFs planar manipulators in the current work. Hence, extension of the developed controllers to the general case of planar manipulators with three or more DOFs, or even to the more general case of 6DOFs robotic manipulators, is interesting and deserves to be further studied in the future. Moreover, the developed controllers can be applied only for the fixed camera configuration. With this in mind, how to extend the developed controllers to the case of eye-in-hand camera configuration is another important but extremely challenging research problem to be solved.

Acknowledgment

The authors would like to thank the Associate Editor and the anonymous reviewers for their valuable comments and helpful suggestions to improve the quality of this article. They would also like to thank L. Han, a Ph.D. student in the Autonomous Robot Lab, Shanghai Jiao Tong University, for her valuable help in doing the experiments.

References

[1] F. Chaumette and S. A. Hutchinson, "Visual servo control—Part I: Basic approaches," *IEEE Robot. Autom. Mag.*, vol. 13, no. 4, pp. 82–90, Dec. 2006.

[2] R. Kelly, "Robust asymptotically stable visual servoing of planar robots," *IEEE Trans. Robot. Autom.*, vol. 12, no. 5, pp. 759–766, Oct. 1996.

[3] G. Hu, N. Gans, N. Fitz-Coy, and W. E. Dixon, "Adaptive homography-based visual servo tracking control via a quaternion formulation," *IEEE Trans. Control Syst. Technol.*, vol. 18, no. 1, pp. 128–135, Jan. 2010.

[4] H. Gu, H. Wang, F. Xu, Z. Liu, and W. Chen, "Active fault detection of soft manipulator in visual servoing," *IEEE Trans. Ind. Electron.*, early access, Oct. 9, 2020, doi: 10.1109/TIE.2020.3028813.

[5] L. Han, H. Wang, Z. Liu, W. Chen, and X. Zhang, "Vision-based cutting control of deformable objects with surface tracking," *IEEE/ASME Trans. Mechatron.*, early access, Oct. 6, 2020, doi: 10.1109/TMECH.2020.3029114.

[6] J. Chen, B. Jia, and K. Zhang, "Trifocal tensor-based adaptive visual trajectory tracking control of mobile robots," *IEEE Trans. Cybern.*, vol. 47, no. 11, pp. 3784–3798, Nov. 2017.

[7] B. Li, X. Zhang, Y. Fang, and W. Shi, "Visual servoing of wheeled mobile robots without desired images," *IEEE Trans. Cybern.*, vol. 49, no. 8, pp. 2835–2844, Aug. 2019.

[8] K. Zhang, J. Chen, Y. Li, and X. Zhang, "Visual tracking and depth estimation of mobile robots without desired velocity information," *IEEE Trans. Cybern.*, vol. 50, no. 1, pp. 361–373, Jan. 2020.

[9] J. Gao, A. A. Proctor, Y. Shi, and C. Bradley, "Hierarchical model predictive image-based visual servoing of underwater vehicles with adaptive neural network dynamic control," *IEEE Trans. Cybern.*, vol. 46, no. 10, pp. 2323–2334, Oct. 2016.

[10] K. Hosoda and M. Asada, "Versatile visual servoing without knowledge of true jacobian," in *Proc. IEEE/RSJ Int. Conf. Intell. Robots Syst.*, Munich, Germany, 1994, pp. 186–193.

[11] M. Jagersand, O. Fuentes, and R. Nelson, "Experimental evaluation of uncalibrated visual servoing for precision manipulation," in *Proc. IEEE Int. Conf. Robot. Autom.*, Albuquerque, NM, USA, 1997, pp. 2874–2880.

[12] H. Sutanto, R. Sharma, and V. Varma, "The role of exploratory movement in visual servoing without calibration," *Robot. Auton. Syst.*, vol. 23, no. 3, pp. 153–169, 1998.

[13] J. A. Piepmeier, G. V. McMurray, and H. Lipkin, "Uncalibrated dynamic visual servoing," *IEEE Trans. Robot. Autom.*, vol. 20, no. 1, pp. 143–147, Feb. 2004.

[14] J. A. Piepmeier and H. Lipkin, "Uncalibrated eye-in-hand visual servoing," *Int. J. Robot. Res.*, vol. 22, nos. 10–11, pp. 805–819, 2003.

[15] A. Shademan, A. M. Farahmand, and M. Jagersand, "Robust Jacobian estimation for uncalibrated visual servoing," in *Proc. IEEE Int. Conf. Robot. Autom.*, Albuquerque, NM, USA, 2010, pp. 5564–5569.

[16] P. Jiang, L. C. A. Bamforth, Z. Feng, J. E. F. Baruch, and Y. Chen, "Indirect iterative learning control for a discrete visual servo without a camera-robot model," *IEEE Trans. Syst., Man, Cybern. B, Cybern.*, vol. 37, no. 4, pp. 863–876, Aug. 2007.

[17] M. Hao and Z. Sun, "A universal state-space approach to uncalibrated model-free visual servoing," *IEEE/ASME Trans. Mechatron.*, vol. 17, no. 5, pp. 833–846, Oct. 2012.

[18] J. Su, H. Ma, W. Qiu, and Y. Xi, "Task-independent robotic uncalibrated hand-eye coordination based on the extended state observer," *IEEE Trans. Syst., Man, Cybern. B, Cybern.*, vol. 34, no. 4, pp. 1917–1922, Aug. 2004.

[19] A. M. Farahmand, A. Shademan, and M. Jagersand, "Global visual-motor estimation for uncalibrated visual servoing," in *Proc. IEEE/RSJ Int. Conf. Intell. Robots Syst.*, San Diego, CA, USA, 2007, pp. 1969–1974.

[20] J. Su, Y. Xi, U. D. Hanebeck, and G. Schmidt, "Nonlinear visual mapping model for 3-D visual tracking with uncalibrated eye-in-hand robotic system," *IEEE Trans. Syst., Man, Cybern. B, Cybern.*, vol. 34, no. 1, pp. 652–659, Feb. 2004.

[21] A. M. Farahmand, A. Shademan, M. Jagersand, and C. Szepesvari, "Model-based and model-free reinforcement learning for visual servoing," in *Proc. IEEE Int. Conf. Robot. Autom.*, Kobe, Japan, 2009, pp. 2917–2924.

[22] Z. Miljkovic, M. Mitic, M. Lazarevic, and B. Babic, "Neural network reinforcement learning for visual control of robot manipulators," *Expert Syst. Appl.*, vol. 40, no. 5, pp. 1721–1736, 2013.

[23] T. Lampe and M. Riedmiller, "Acquiring visual servoing reaching and grasping skills using neural reinforcement learning," in *Proc. Int. Joint Conf. Neural Netw.*, Dallas, TX, USA, 2013, pp. 1–8.

[24] M. Sadeghzadeh, D. Calvert, and H. A. Abdullah, "Self-learning visual servoing of robot manipulator using explanation-based fuzzy neural networks and Q-learning," *J. Intell. Robot. Syst.*, vol. 78, no. 1, pp. 83–104, 2015.

[25] A. X. Lee, S. Levine, and P. Abbeel, "Learning visual servoing with deep features and fitted Q-iteration," in *Proc. Int. Conf. Learn. Represent.*, Toulon, France, 2017, pp. 1–20.

[26] F. Castelli, S. Michieletto, S. Ghidoni, and E. Pagello, "A machine learning-based visual servoing approach for fast robot control in industrial setting," *Int. J. Adv. Robot. Syst.*, vol. 14, no. 6, pp. 1–10, 2017.

[27] A. Saxena, H. Pandya, G. Kumar, A. Gaud, and K. M. Krishna, "Exploring convolutional networks for end-to-end visual servoing," in *Proc. IEEE Int. Conf. Robot. Autom.*, Singapore, 2017, pp. 3817–3823.

[28] Q. Bateux, E. Marchand, J. Leitner, F. Chaumette, and P. I. Corke, "Training deep neural networks for visual servoing," in *Proc. IEEE Int. Conf. Robot. Autom.*, Brisbane QLD, Australia, 2018, pp. 3307–3314.

[29] B. E. Bishop and M. W. Spong, "Adaptive calibration and control of 2D monocular visual servo systems," *Control Eng. Pract.*, vol. 7, no. 3, pp. 423–430, 1999.

[30] E. Zergeroglu, D. M. Dawson, M. S. de Queiroz, and A. Behal, "Vision-based nonlinear tracking controllers with uncertain robot-camera parameters," *IEEE/ASME Trans. Mechatron.*, vol. 6, no. 3, pp. 322–337, Sep. 2001.

[31] A. Astolfi, L. Hsu, M. Netto, and R. Ortega, "A solution to the adaptive visual servoing problem," in *Proc. IEEE Int. Conf. Robot. Autom.*, Seoul, Korea, 2001, pp. 743–748.

[32] A. Astolfi, L. Hsu, M. S. Netto, and R. Ortega, "Two solutions to the adaptive visual servoing problem," *IEEE Trans. Robot. Autom.*, vol. 18, no. 3, pp. 387–392, Jun. 2002.

[33] A. R. L. Zachi, L. Hsu, R. Ortega, and F. Lizarralde, "Cascade control of uncertain manipulator systems through immersion and invariance adaptive visual servoing," in *Proc. IEEE Int. Conf. Robot. Autom.*, New Orleans, LA, USA, 2004, pp. 280–285.

[34] M. R. Akella, "Vision-based adaptive tracking control of uncertain robot manipulators," *IEEE Trans. Robot.*, vol. 21, no. 4, pp. 747–753, Aug. 2005.

[35] R. Ortega and E. Nuno, "New solutions to the 2D adaptive visual servoing problem with relaxed excitation requirements," *Int. J. Adapt. Control Signal Process.*, vol. 33, no. 12, pp. 1843–1856, 2019.

[36] C. C. Cheah, C. Liu, and J. J. E. Slotine, "Adaptive jacobian tracking control of robots with uncertainties in kinematic, dynamic and actuator models," *IEEE Trans. Autom. Control*, vol. 51, no. 6, pp. 1024–1029, Jun. 2006.

[37] C. Liu, C. C. Cheah, and J.-J. E. Slotine, "Adaptive jacobian tracking control of rigid-link electrically driven robots based on visual task-space information," *Automatica*, vol. 42, no. 9, pp. 1491–1501, Sep. 2006.

[38] W. E. Dixon, "Adaptive regulation of amplitude limited robot manipulators with uncertain kinematics and dynamics," *IEEE Trans. Autom. Control*, vol. 52, no. 3, pp. 488–493, Mar. 2007.

[39] X. Liang, X. Huang, M. Wang, and X. Zeng, "Adaptive task-space tracking control of robots without task-space- and joint-space-velocity measurements," *IEEE Trans. Robot.*, vol. 26, no. 4, pp. 733–742, Aug. 2010.

[40] G. Hu *et al.*, "Homography-based visual servo control with imperfect camera calibration," *IEEE Trans. Autom. Control*, vol. 54, no. 6, pp. 1318–1324, Jun. 2009.

[41] Y. H. Liu, H. Wang, C. Wang, and K. K. Lam, "Uncalibrated visual servoing of robots using a depth-independent interaction matrix," *IEEE Trans. Robot.*, vol. 22, no. 4, pp. 804–817, Aug. 2006.

[42] H. Wang, Y. H. Liu, and D. Zhou, "Dynamic visual tracking for manipulators using an uncalibrated fixed camera," *IEEE Trans. Robot.*, vol. 23, no. 3, pp. 610–617, Jun. 2007.

[43] X. Liang, X. Huang, M. Wang, and X. Zeng, "Improved stability results for visual tracking of robotic manipulators based on the depth-independent interaction matrix," *IEEE Trans. Robot.*, vol. 27, no. 2, pp. 371–379, Apr. 2011.

[44] H. Wang, Y.-H. Liu, and D. Zhou, "Adaptive visual servoing using point and line features with an uncalibrated eye-in-hand camera," *IEEE Trans. Robot.*, vol. 24, no. 4, pp. 843–857, Aug. 2008.

[45] C. C. Cheah, C. Liu, and J. J. E. Slotine, "Adaptive Jacobian vision based control for robots with uncertain depth information," *Automatica*, vol. 46, no. 7, pp. 1228–1233, 2010.

[46] H. Wang, "Adaptive visual tracking for robotic systems without image-space velocity measurement," *Automatica*, vol. 55, pp. 294–301, May 2015.

[47] X. Liang, H. Wang, Y.-H. Liu, W. Chen, and J. Zhao, "A unified design method for adaptive visual tracking control of robots with eye-in-hand/fixed camera configuration," *Automatica*, vol. 59, pp. 97–105, Sep. 2015.

[48] X. Liang, H. Wang, Y.-H. Liu, W. Chen, and Z. Jing, "Image-based position control of mobile robots with a completely unknown fixed camera," *IEEE Trans. Autom. Control*, vol. 63, no. 9, pp. 3016–3023, Sep. 2018.

[49] X. Liang, H. Wang, Y.-H. Liu, B. You, Z. Liu, and W. Chen, "Calibration-free image-based trajectory tracking control of mobile robots with an overhead camera," *IEEE Trans. Autom. Sci. Eng.*, vol. 17, no. 2, pp. 933–946, Apr. 2020.

[50] X. Liang *et al.*, "Purely image-based pose stabilization of nonholonomic mobile robots with a truly uncalibrated overhead camera," *IEEE Trans. Robot.*, vol. 36, no. 3, pp. 724–742, Jun. 2020.
[51] C. C. Cheah, "Task-space PD control of robot manipulators: Unified analysis and duality property," *Int. J. Robot. Res.*, vol. 27, no. 10, pp. 1152–1170, 2008.

Xinwu Liang (Member, IEEE) received the B.S. and Ph.D. degrees in control engineering from the Huazhong University of Science and Technology, Wuhan, China, in 2006 and 2011, respectively.

He was a Postdoctoral Fellow with the Department of Automation, Shanghai Jiao Tong University, Shanghai, China, from 2011 to 2014, and the Department of Mechanical and Automation Engineering, The Chinese University of Hong Kong, Hong Kong, from 2014 to 2015. He is currently an Associate Professor with the School of Aeronautics and Astronautics, Shanghai Jiao Tong University. His current research interests include robot control, visual servoing, vision-based navigation, adaptive control, and computer vision.

Hesheng Wang (Senior Member, IEEE) received the B.Eng. degree in electrical engineering from the Harbin Institute of Technology, Harbin, China, in 2002, and the M.Phil. and Ph.D. degrees in automation and computer-aided engineering from The Chinese University of Hong Kong, Hong Kong, in 2004 and 2007, respectively.

He was a Postdoctoral Fellow and a Research Assistant with the Department of Mechanical and Automation Engineering, The Chinese University of Hong Kong, from 2007 to 2009. He is currently a Professor with the Department of Automation, Shanghai Jiao Tong University, Shanghai, China. His current research interests include visual servoing, service robots, and autonomous driving.

Prof. Wang is an Associate Editor of *Assembly Automation* and the *International Journal of Humanoid Robotics*, and a Technical Editor of the IEEE/ASME TRANSACTIONS ON MECHATRONICS. He served as an Associate Editor of the IEEE TRANSACTIONS ON ROBOTICS from 2015 to 2019. He was the General Chair of the IEEE Real-Time Computing and Robotics in 2016, and the Program Chair of the IEEE Robotics and Biomimetics in 2014 and IEEE/ASME Advanced Intelligent Mechatronics in 2019.

Yun-Hui Liu (Fellow, IEEE) received the B.Eng. degree in applied dynamics from the Beijing Institute of Technology, Beijing, China, in 1985, the M.Eng. degree in mechanical engineering from Osaka University, Osaka, Japan, in 1989, and the Ph.D. degree in mathematical engineering and information physics from the University of Tokyo, Tokyo, Japan, in 1992.

He was with the Electrotechnical Laboratory, Ministry of International Trade and Industry, Ibaraki, Japan, from 1992 to 1995. Since 1995, he has been with The Chinese University of Hong Kong (CUHK), Hong Kong, where he is currently a Choh-Ming Li Professor of Mechanical and Automation Engineering and the Director of CUHK T Stone Robotics Institute. He is also visiting the State Key Laboratory of Robotics Technology and Systems, Harbin Institute of Technology, Harbin, China, and the Director of the Joint Centre for Intelligent Sensing and Systems, National University of Defense Technology, Hunan, China, and CUHK. He has published over 200 papers in refereed journals and refereed conference proceedings. His current research interests include visual servoing, medical robotics, multifingered robot hands, mobile robots, sensor networks, and machine intelligence.

Dr. Liu was a recipient of numerous research awards from international journals and international conferences in robotics and automation and government agencies and was listed in the Highly Cited Authors (Engineering) by Thomson Reuters in 2013. He is the Editor-in-Chief of *Robotics and Biomimetics* and an Editor of *Advanced Robotics*. He served as an Associate Editor of the IEEE TRANSACTIONS ON ROBOTICS AND AUTOMATION and the General Chair of the 2006 IEEE/RSJ International Conference on Intelligent Robots and Systems.

Bing You received the B.S. and M.S. degrees in control engineering from the Huazhong University of Science and Technology, Wuhan, China, in 2006 and 2008, respectively.

He is currently a Senior Control System Engineer with the Maintenance Department III, Fujian Fuqing Nuclear Power Company Ltd., Fuqing, China. His current research interests include automation control systems, application of robots in nuclear power plants, and cybersecurity of industry Internet.

Zhe Liu received the B.S. degree in automation from Tianjin University, Tianjin, China, in 2010, and the Ph.D. degree in control technology and control engineering from Shanghai Jiao Tong University, Shanghai, China, in 2016.

From 2017 to 2020, he was a Postdoctoral Fellow with the Department of Mechanical and Automation Engineering, The Chinese University of Hong Kong, Hong Kong. He is currently a Research Associate with the Department of Computer Science and Technology, University of Cambridge, Cambridge, U.K. His current research interests include autonomous mobile robots, multirobot cooperation, and autonomous driving systems.

Zhongliang Jing (Senior Member, IEEE) received the B.S., M.S., and Ph.D. degrees in electronics and information technology from Northwestern Polytechnical University, Xi'an, China, in 1983, 1988, and 1994, respectively.

He was a Research Associate and a Senior Visiting Scholar with the University of California at Berkeley, Berkeley, CA, USA, from 1997 to 1998. He is currently a Cheung Kong Professor with the School of Aeronautics and Astronautics, Shanghai Jiao Tong University, Shanghai, China, where he has been the Director of the Engineering Research Center of Aerospace Science and Technology, Ministry of Education of the People's Republic of China since 2013, and the Shanghai Collegiate Key Laboratory of Aerospace Science and Technology since 2014. He has published over 200 journal papers and seven monographs. His current research interests include adaptive filtering, target tracking, information fusion, avionics integration, and soft robot control.

Dr. Jing is currently the Editor-in-Chief of the *Aerospace Systems* (Springer). He has been the Editorial Board Member of several journals, such as the *International Journal of Space Science and Engineering*, *Information and Control*, *Systems Engineering and Electronics*, and *Manned Spaceflight*.

Weidong Chen (Member, IEEE) received the B.S. and M.S. degrees in control engineering and the Ph.D. degree in mechatronics from the Harbin Institute of Technology, Harbin, China, in 1990, 1993, and 1996, respectively.

Since 1996, he has been with the Shanghai Jiao Tong University, Shanghai, China, where he is currently a Professor with the Department of Automation and the Deputy Dean of the Institute of Medical Robotics. He is the Founder of the Autonomous Robot Laboratory. From 2013 to 2019, he served as the Chair of the Department of Automation. He has also been recognized by the New Century Excellent Talents with the University of the Ministry of Education of China in 2007 and a Shanghai Shuguang Scholar in 2004. His current research interests include perception and control of robotic systems, multirobot systems, and medical robotics.